Epidemiological and ecological determinants of Zika virus transmission in an urban setting.

Lourenço J[1,*], Maia de Lima M[3], Faria NR[1], Walker AS[1], Kraemer MUG[1], Villabona-Arenas CJ[4], Lambert B[1], Marques de Cerqueira E[2], Pybus OG[1], Alcantara LCJ[3], Recker M[5],

[1] Department of Zoology, University of Oxford, Oxford OX1 3PS, UK

[2] Centre of PostGraduation in Collective Health, Department of Health, Universidade Estadual de Feira de Santana, Feira de Santana, Bahia, Brazil.

[3] FIOCRUZ, Laboratory of Haematology, Genetics and Computational Biology, Salvador, Bahia, Brazil.

[4] Institut de Recherche pour le Développement (IRD), UMI 233, INSERM U1175 and Institut de Biologie Computationnelle, LIRMM, Université de Montpellier, Montpellier, France.

[5] Centre for Mathematics and the Environment, University of Exeter, Penryn Campus, Penryn TR10 9FE, UK

[*] Corresponding author: jose.lourenco@zoo.ox.ac.uk

Abstract

The Zika virus has emerged as a global public health concern. Its rapid geographic expansion is attributed to the success of *Aedes* mosquito vectors, but local epidemiological drivers are still poorly understood. Feira de Santana played a pivotal role in the Chikungunya epidemic in Brazil and was one of the first urban centres to report Zika infections. Using a climate-driven transmission model and notified Zika case data, we show that a low observation rate and high vectorial capacity translated into a significant attack rate during the 2015 outbreak, with a subsequent decline in 2016 and fade-out in 2017 due to herd-immunity. We find a potential Zika-related, low risk for microcephaly per pregnancy, but with significant public health impact given high attack rates. The balance between the loss of herd-immunity and viral re-importation will dictate future transmission potential of Zika in this urban setting.

Introduction

The first cases of Zika virus (ZIKV) in Brazil were concurrently reported in March 2015 in Camaçari city in the state of Bahia [1] and in Natal, the state capital city of Rio Grande do Norte [2]. During that year, the epidemic in Camaçari quickly spread to other municipalities of the Bahia state, including the capital city of Salvador, which together accounted for over

90% of all notified Zika cases in Brazil in 2015 [3]. During this period, many local Bahia health services were overwhelmed by an ongoing Chikungunya virus (CHIKV, East Central South African genotype) epidemic, that was first introduced in 2014 in the city of Feira de Santana (FSA) [4, 5]. The role of FSA in the establishment and subsequent spread of CHIKV highlights the importance of its socio-demographic and climatic setting, which may well be representative for the transmission dynamics of arboviral diseases in the context of many other urban centres in Brazil and around the world.

On the 1^{st} February 2015 the first ZIKV cases were reported in FSA, followed by a large epidemic that continued into 2016. The rise in ZIKV incidence in FSA coincided temporally with an increase in cases of Guillain-Barré syndrome (GBS) and microcephaly [3], with an unprecedented total of 21 confirmed cases of microcephaly in FSA between January 2015 and May 2017. There is wide statistical support for a causal link between ZIKV and severe manifestations such as microcephaly [6, 7, 8, 9, 10, 11], and the proposed link in 2015 led to the declaration of the South American epidemic as an international public health emergency by the World Health Organization (WHO) in 2016; the response to which has been limited to vector control initiatives and advice to delay pregnancy in the affected countries [12, 13]. With few cohort studies published [9, 10] and the lack of an established experimental model for ZIKV infection [14, 15], modelling efforts have taken a central role for advancing our understanding of the virus's epidemiology [16, 17, 18, 19, 20, 21, 22]. In particular, our knowledege on parameters of public health importance, such as the basic reproduction number (R_0), the duration of infection [17], attack and reporting rates [23], the risk of sexual transmission [24, 25, 26] and birth-associated microcephaly [27, 21] has advanced significantly from studies using transmission models. Climate variables are critical for the epidemiological dynamics of Zika and other arboviral diseases, such as dengue [28, 29, 30, 31] and chikungunya [32, 33, 34]. Although these have also been previously addressed in mapping and / or modelling studies (e.g. [18, 20, 21, 22]), their effects as ecological drivers for the emergence, transmission and endemic potential of the Zika virus, especially in the context of a well described outbreak, have not yet been addressed in detail.

In this study, focusing on an urban centre of Brazil (Feira de Santana), we explicitly model the mosquito-vector lifecycle under seasonal, weather-driven variations. Using notified case data of both the number of suspected Zika infections and confirmed microcephaly cases, we demonstrate how the combination of high suitability for viral transmission and a low detection rate resulted in an extremely high attack rate during the first epidemic wave in 2015. The rapid accumulation of herd-immunity significantly reduced the number of cases during the following year, when total ZIKV-associated disease was peaking at the level of the country. Projecting forward we find that the demographic loss of herd-immunity together with the frequency of reintroduction will dictate the risk of reemergence and endemic establishment of Zika in Feira de Santana. The conclusions of this study should be transferable to major urban centres of Brazil and elsewhere with similar climatic and demographic settings.

Methods Summary

To model the transmission dynamics of ZIKV infections and estimate relevant epidemiological parameters, we fitted an ento-epidemiological, climate-driven transmission model to ZIKV incidence and climate data of FSA between 2015 and 2017 within a Bayesian framework, similar to our previous work on a dengue outbreak in the Island of Madeira [28].

The model is based on ordinary differential equations (ODE) describing the dynamics of viral infections within the human and mosquito populations (eqn. 1-5 and 6-10, respectively). The human population is assumed to be fully susceptible before the introduction of ZIKV and is kept constant in size throughout the period of observation. After an infectious mosquito bite, individuals first enter an incubation phase, after which they become infectious to a mosquito for a limited period of time. Fully recovered individuals are assumed to retain life-long immunity. We assumed that sexual transmission did not significantly contribute to transmission dynamics and therefore ignored its effects [35, 26, 24].

For the dynamics of the vector populations we divided mosquitoes into two life-stages: aquatic and adult females. Adult mosquitoes were further divided into the epidemiologically relevant stages for arboviral transmission: susceptible, incubating and infectious. In contrast to human hosts, mosquitoes remain infectious for life. The ODE model comprised 8 climate-dependent entomological parameters (aquatic to adult transition rate, aquatic mortality rate, adult mortality rate, oviposition rate, incubation period, transmission probability to human, hatching success rate and biting rate), whose dependencies on temperature, rainfall and humidity were derived from other studies (see Table 2).

Four parameters (baseline mosquito biting rate, mosquito sex ratio, probability of transmission from human-to-vector and human lifespan) were fixed to their expected mean values, taken from the literature (see Table 3). To estimate the remaining parameters, alongside parameter distributions regarding the date of first infection, the human infectious and incubating periods, and the observation rate of notified ZIKV cases, we fitted the ODE model to weekly notified cases of ZIKV in FSA using a Bayesian Markov-chain Monte Carlo (MCMC) approach. The results are presented both in terms of mean dynamic behaviour of the ODE under the MCMC solutions and posterior distributions of key epidemiological parameters. A full description of the fitting approach and the estimated parameters can be found in the section *Materials and Methods*.

Results

On the 1^{st} February 2015 the first Zika virus (ZIKV) case was reported in Feira de Santana (FSA). Weekly cases remained very low for the following two months, adding up to just 10 notified cases by the end of March that year (Figure 1A). A rapid increase in the number of cases was observed in April, coinciding with Micareta, a local carnival-like festival that takes place across the urban centres of Bahia. The epidemic peaked in July 2015, which was followed by a sharp decline in notified cases over the next 1-2 months. This first epidemic wave was followed by a significantly smaller outbreak in 2016, peaking around March, and an even smaller outbreak in 2017 with no discernable epidemic peak.

Confirmed (and monthly aggregated) microcephaly (MC) cases were absent by November 2015, after which a small epidemic was observed with peak counts in January 2016. We found a time lag of 5-6 months (20-24 weeks) between the first reported Zika epidemic wave and the MC peak in case counts. This coincides with previous observations suggesting a link between the development of neurological complications in newborns and ZIKV infection during the second trimester [3]. We note that our lag may be offset by around 1-4 weeks, however, since the date of MC cases in our dataset represents the date of diagnostic confirmation, which is usually done postpartum.

Overall, the epidemic behaviour in FSA was in sharp contrast with trends observed in notified cases across Brazil (BR) as a whole, for which the second epidemic in 2016 was approximately 6 times larger than the one in 2015 (Figure 1A), suggesting the Bahia state as a focus point in the emergence and initial spread of ZIKV in Brazil [36, 3]. Nonetheless, a clear temporal synchronization between country level and FSA case counts could be observed.

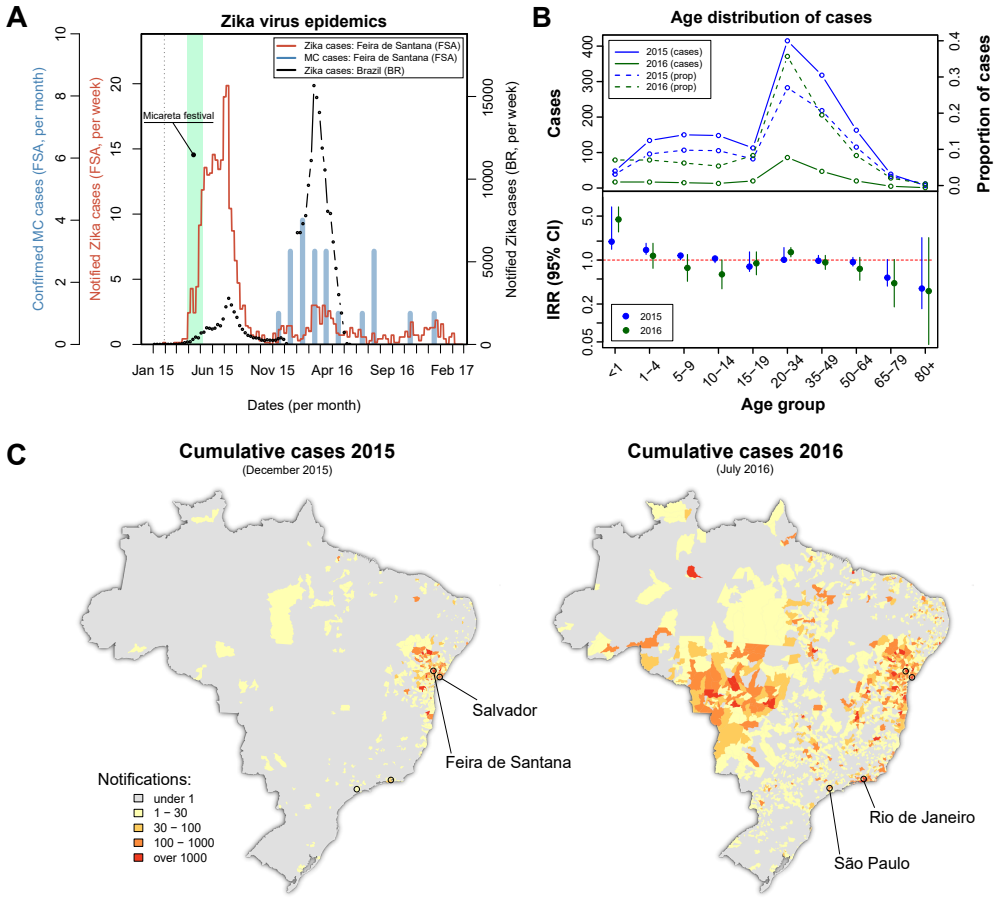

Figure 1 - Zika virus epidemics in Feira de Santana and Brazil (2015-2016). *(A)* Comparison of weekly notified Zika cases (full red line) with monthly Microcephaly cases (blue bars) in Feira de Santana (FSA), overimposed with total Zika cases at the level of the country (BR, black dotted line). BR data for weeks 50-52 was missing. Green area

highlights the time period for the Micareta festival and the dotted grey line the date of first notification. Incidence series is available as Dataset 3 and Microcephaly series as Dataset 4. *(B)* Age distribution and incidence rate ratio (IRR) for the 2015 (blue) and 2016 (green) FSA epidemics (data available as Dataset 2). The top panel shows the number of cases per age (full lines) and the proportion of total cases per age class (dashed lines), which peak at the age range 20-50. The bottom panel shows the age-stratified incidence risk ratio (IRR, plus 95% CI), with the red dotted line indicating $IRR = 1$. *(C)* Spatial distribution of cumulative notified cases in BR at the end of 2015 (left) and mid 2016 (right). Two largest urban centres in the Bahia state (Salvador, Feira de Santana) and at the country level (São Paulo, Rio de Janeiro) are highlighted.

The age distribution of notified ZIKV cases in FSA suggested a higher proportion of cases between 20 and 50 years of age, but with no discernible differences between the two epidemics (Figure 1B, top panel). However, when corrected for the expected number of cases assuming an equal risk of infection per age class, we found the number of cases within this age group to be closer to most other groups (incidence rate ratio, IRR, close to 1, Figure 1B, bottom panel). The per capita case counts within the youngest age class (<1 years) appeared higher than expected, with an IRR significantly above 1 and also higher in 2016 (IRR=4.4, 95% CI [2.8, 7.0]) than in 2015 (IRR=1.95, 95% CI [1.5, 2.6]), possibly indicating biased reporting and / or health care seeking with increased awareness of the disease. There was also a consistent trend towards reduced IRR in the elderly (>65 years), although with significant uncertainties. Finally, a small increase in IRR could be detected in the 20-34 year olds, which could potentially be a signature of sexual transmission in this age group [25, 37, 38, 39, 35, 24, 26]. At this stage and without more detailed data it was not possible to ascertain whether these findings indicated age-related risk of disease, age-dependent exposure risk or simply notification biases in particular age groups, however.

The spatial distribution of total notified cases for BR highlighted the expected clustering of ZIKV cases within the Bahia state by the end of 2015 as well as the wider geographical range by July 2016 (Figure 1C). We speculate that the difference in geographical range could explain the higher number of cases observed during the 2016 epidemic at the country level. This, on the other hand, did not explain why the second epidemic in FSA was nearly 7 times smaller than the first and with only sporadic cases in 2017. To answer this question and to obtain robust parameter estimates of ZIKV epidemiological relevance we utilised a dynamic transmission model, which we fitted to notified case data and local climate variables of FSA within a Bayesian framework (see Materials and Methods).

Climate-driven vectorial capacity

The reliance on *Aedes* mosquitoes for transmission implies that the transmission potential of ZIKV is crucially dependent on temporal trends in the local climate. We therefore investigated daily rainfall, humidity and mean temperature data in FSA between 2013 and May 2017 (Figure 2A). The data showed erratic fluctuations in rainfall with sporadic episodes of intense rain but without a clear seasonal trend. Temperature, on the other hand, presented a much clearer seasonal signature with fixed amplitudes between 22 and 27 degree Celsius, peaking between December and May. Humidity showed an intermediate

scenario and appeared correlated with periods of intense rainfall but negatively correlated with temperature.

By fitting our climate-driven transmission model to the local climate and ZIKV case data (see Material and Methods and Figure 2B) we obtained parameter estimates for the mosquito lifespan as well as the viral extrinsic incubation period (EIP) for the same period. Mosquito lifespan and EIP are main drivers of vectorial capacity and both showed seasonal oscillations with median values of around 9 and 5 days, respectively (Figure 8), which are in line with ranges found in the literature ([40, 41, 42, 43] and Table 1). Importantly, there was a strong negative temporal correlation between these two variables, with periods of longer EIP coinciding with shorter lifespans and vice-versa. This negative relationship resulted in large temporal variations in vectorial capacity and thus seasonal oscillations in the daily reproductive numbers, R_0, with a median value of 2.7 in the period 2015-2017 (range 1.0-4.3, Figure 8), and 2.2 before 2015, peaking in the local summer months between December and April (Figure 2C). Importantly, R_0 remained above 1 for the entire period, indicating a high suitability for ZIKV in FSA. It should be noted that R_0 in this context is a time-dependent variable, i.e. $R_0(t)$, but out of convenience we simply refer to it as R_0.

We also looked at the relationship between each climatic variable and R_0 and case counts (Figures 2D and E, respectively). The transmission potential was strongly and positively correlated with temperature ($r^2 = 0.728$) and negatively with humidity ($r^2 = 0.26$). As expected, from the highly random patterns in the climate series, there was no correlation between R_0 and rainfall ($r^2 = 0.008$). In contrast, there was an opposite trend in the relationship between the climatic variables and case counts, with a positive correlation with humidity ($r^2 = 0.28$) and a negative correlation with temperature ($r^2 = 0.23$). As with R_0 there was only a weak observable trend in the relationship between rainfall and the number of Zika cases. It should be understood that this macroscopic analysis does not take into account the expected temporal lags due to mosquito development, incubation periods etc., so the purpose here was simply to identify a general qualitative relationship between climate, vectorial capacity and disease incidence.

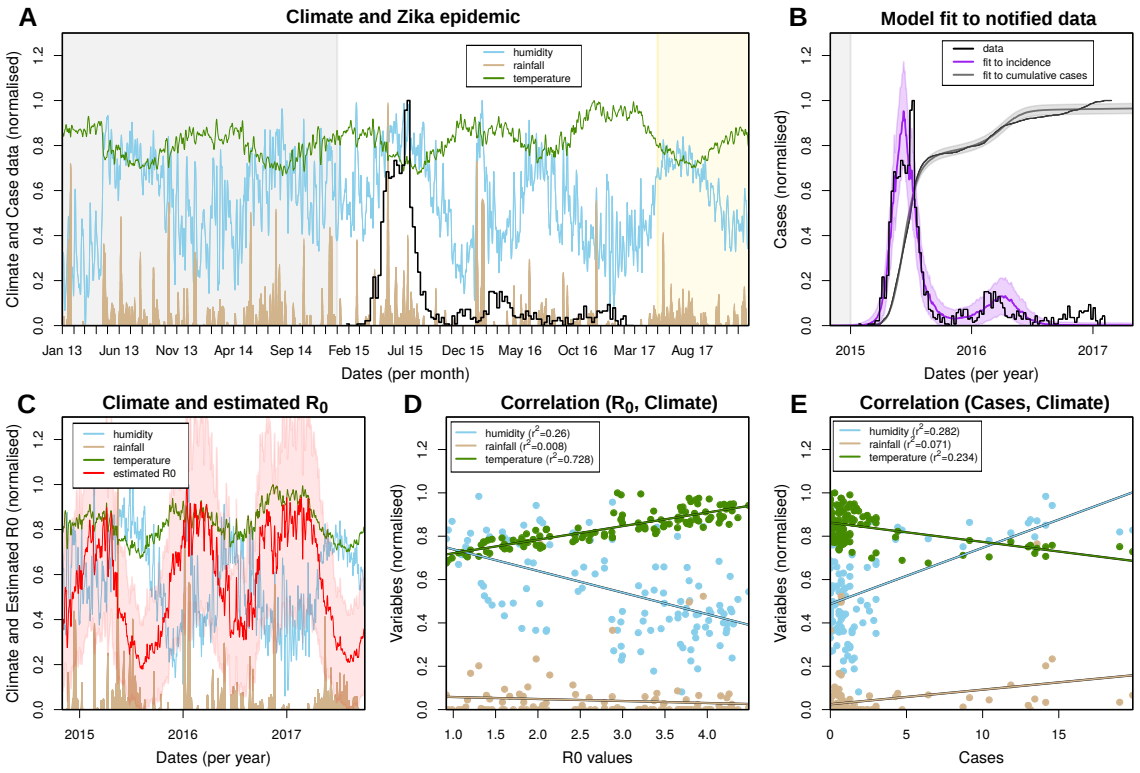

Figure 2 - Eco-epidemiological factors and model fit to notified cases. *(A)* Zika case data (black) and daily climatic series for rainfall (gold), humidity (blue) and mean temperature (green) for Feira de Santana (FSA). Climate data available as Dataset 1. *(B)* Resulting Bayesian MCMC fit to weekly (black line: data, purple line: model fit) and cumulative incidence (black line: data, grey line: model fit). *(A,B)* The grey areas highlight the period before the Zika outbreak, the white areas highlight the period for which notified case data was available, and the yellow shaded areas highlight the period for which mean climatic data was used (see Materials and Methods). *(C)* Climatic series as in *A* and estimated R_0 for the period of the outbreak (2015-2017) (R_0 absolute values in Figure 8). *(D)* Correlations between the estimated R_0 and climatic variables (intercepts: 0.839 for humidity, 0.067 for rainfall and 0.658 for temperature). *(E)* Correlations between the case counts and climatic variables (intercepts: 0.487 for humidity, 0.024 for rainfall and 0.862 for temperature). *(D,E)* Points presented are from timepoints (weeks) for which incidence was notified. *(A-E)* Y-axis normalised between 0 and 1 for visualisation purposes.

Model fit and parameter estimates

Four parameters of public health importance were estimated by our MCMC framework: the date of introduction, the human infectious period, the human (intrinsic) incubation period, and the case observation rate (Table 4). The posterior for the introduction date showed a strong support for an introduction into FSA in early-mid December 2014 (estimated median: 10^{th} of December), i.e. around 7-8 weeks before the first notified case (Figure 3A). The estimated human infectious period was $\approx$ 6 days (Figure 3C, median= 5.9, 95% CI

[5.47-6.14]), which was very similar to the estimated incubation period (Figure 3D, median= 5.8, 95% CI [5.6-6.15]) and in line with previously estimated ranges for ZIKV (Table 1). In this context it is important to note that informative priors had been used for these 2 parameters (Figure 7), and the posterior for the incubation period presented an adjustment of ≈ -0.5 days relative to the proposed distribution from the literature.

Of particular interest here was the very low observation rate (Figure 3B), with a median of just under 0.004 (median= 0.0039, 95% CI [0.0038-0.0041]), which equates to less than 4 in 1000 infections having been notified during the epidemic in FSA. Although lower than other previously reported estimates, this would explain the relatively long period of low viral circulation before the epidemic took off in April 2015. That is, based on our estimates, there were around 2,700 Zika infections during the first 2 months, of which only 10 were notified. More importantly, when applying this rate to the total number of cases we found that by the end of the first epidemic wave around 65% (95% CI [57.0-72.9]) of the population in FSA had been infected by the virus. This high attack rate is not unusual for Zika, however, and is in general agreement with observations elsewhere (Table 1).

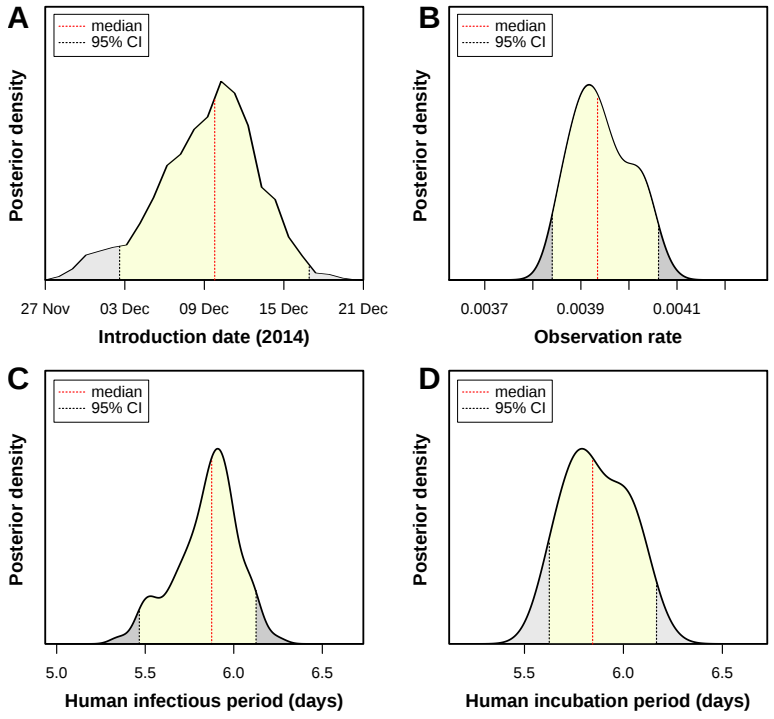

Figure 3 - Estimated epidemiological and ecological parameters. MCMC posterior distributions, based on model fitting to notified case data between 2015-2017 and obtained from sampling 1 million MCMC steps after burn-in. *(A)* Posterior of the introduction date with median 10^{th} December 2014 (95% CI [01-16 Dec]). *(B)* Posterior of the observation rate with median 0.0039 (95% CI [0.0038-0.0041])). *(C)* Posterior of the human infectious period with median 5.9 days (95% CI [5.47-6.14]). *(D)* Posterior of the human (intrinsic) incubation period with median 5.8 days (95% CI [5.6-6.15]). Representative samples of 500 MCMC chain states are available in Supplementary Files 1-6. See Figure 9 for sample chain behaviour.

Future transmission potential for Zika virus

As illustrated by the cumulative attack rate in Figure 4A, and similar to estimates from other regions in the world (Table 1), nearly 65% of the population got infected by ZIKV by the end of 2015, which rose to over 75% (95% CI [76.9-84.3]) by the end of 2016. During the first wave most cases occurred off-season, here defined by our estimated daily reproductive number (R_0), while the second wave appeared much more synchronized with the period of high transmission potential. Notably, this temporal phenomenon has also been observed for the chikungunya virus (CHKV) when it was first introduced into FSA in 2014 [5].

The amassed accumulation of herd-immunity during the first wave resulted in a marked difference between the estimated basic reproductive number, R_0, and the effective reproductive ratio (R_e) by the end of 2015 (Figure 4A). This in turn might explain the marked reduction in Zika cases in FSA in 2016, at a time when the virus was infecting large numbers of individuals elsewhere in the country (Figures 1A, C). At the start of 2016, R_e was estimated to be more than 3 times smaller than R_0, which increased to 5 by the beginning of 2017. Projecting into the future using average climate data for this region showed that the mean effective reproductive number is expected to remain low and close to 1 for the next few years, suggesting a very weak potential for ZIKV endemicity in the near future. In fact, the sporadic nature of Zika cases in 2017 strongly suggest that herd immunity in this region is at a sufficiently high level to prevent sustained transmission. Furthermore, during 2017, R_e was on average less than 1 (mean: 0.62, range: 0.25-1.06), and we would therefore argue that the small number of cases (1.4% of 2015-2017) were mostly a result of small transmission chains, either from resonant transmission from the previous year, or from introduction events from nearby locations. Crucially, this would also explain why our ODE model matched both the dynamics and the sizes of the first two epidemic waves in FSA between 2015 and 2016 but failed to capture the small number of cases during 2017 (Figure 2B).

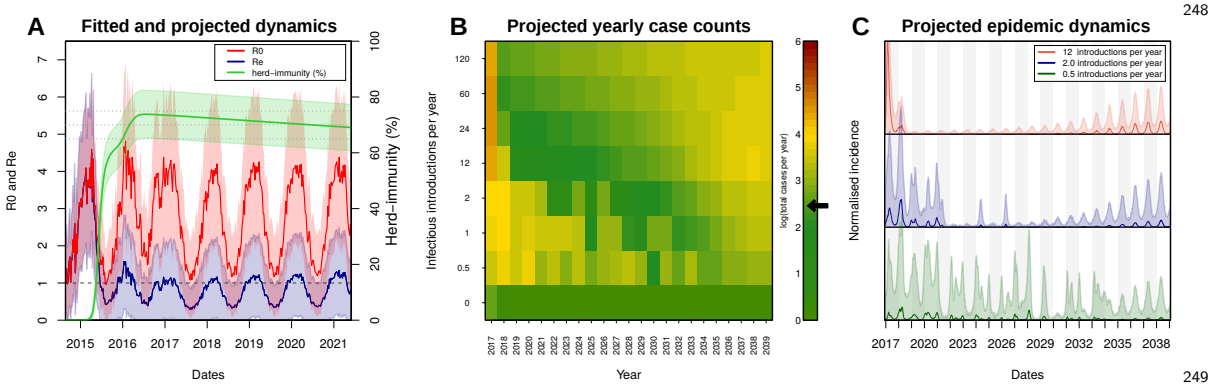

Figure 4 - Projected Zika virus dynamics and transmission potential. *(A)* Fitted and projected epidemic attack rate (% population infected, or herd-immunity, green), basic reproduction number (R_0, red) and effective reproduction number (R_e, blue).*(B)* Colourmap showing the projected total number of annual cases depending on rate of external introduction of infectious individuals.The black arrow in the color scale marks the total

number of real cases necessary for 1 notified case to be reported in FSA. *(C)* Projected incidence dynamics when considering less than 1 (green), 2 (blue) and 12 (red) external introductions per year. Grey and white shaded areas delineate different years. The Y-axes are normalised to 1 in each subplot for visualisation purposes. In *(B, C)* results are based on 1000 stochastic simulations with parameters sampled from the posterior distributions (Figure 3). Representative model solutions for incidence, R0 and Re from 500 MCMC chain samples are available in Supplementary Files 1-6 (both deterministic and stochastic).

Without external introductions of infectious individuals (human or vector) our results predicted an epidemic fade-out by 2017, in accordance with the lack of notified cases after March 2017 (Figure 4A). We therefore projected ZIKV's epidemic potential over the next two decades (until 2040) using stochastic simulations (see Material and Methods) while assuming different rates of viral introduction (Figures 4B, C). Our results showed that the potential for ZIKV to cause another outbreak or to establish itself endemically in FSA is strongly dependent on the frequency of re-introductions, whereby higher rates of external introductions might in fact help to sustain high levels of herd immunity, whereas infrequent introductions are more likely to result in notable outbreaks. That is, semi-endemic behaviour was only observed in simulations with low introduction rates (Figures 4B-C), as these scenarios strike a fine balance between a low number of new cases affecting herd-immunity levels and population turnover. In contrast, high introduction rates quickly exhaust the remaining susceptible pool, resulting in very long periods without epidemic behaviours.

Sensitivity to reporting and microcephaly risk

In effect, our estimated observation rate entails the proportion of real infections that would have been notified if symptomatic and correctly diagnosed as Zika. Based on the previously reported Yap Island epidemic of 2007 [44], the percentage of symptomatic infections can be assumed to be close to 18%. Unfortunately, measures of the proportion of individuals seeking medical attention and being correctly diagnosed do not exist for FSA, although it is well known that correct diagnosis for DENV is imperfect in Brazil [45]. We therefore performed a sensitivity analysis by varying both the proportions of infected symptomatic individuals seeking medical attention and the proportion of those being correctly diagnosed for Zika. Figure 5A shows that if any of these proportions is less than 10%, or both between 15-20%, our observation rate of 3.9 per 1000 infections can easily be explained.

Finally we investigated the sensitivity of our results with regards to the expected number of newborns presenting microcephaly (MC). Following the observation that virtually all reported MC cases were issued before the summer of 2016 and with a lag of 5-6 months (Figure 1A), we assumed that the vast majority of Zika-associated MC cases would have been a consequence of the first epidemic wave in 2015. We used the estimated attack rate of approximately 65% from 2015 (Figure 4A) and varied the local birth rate and the theoretical risk of MC to obtain an expected number of cases. In agreement with other reports [7, 46, 47, 48], our model predicted a relatively low risk for MC given ZIKV infection during pregnancy (Figures 5B, C). In particular, using a conservative total of 21 confirmed MC cases in FSA, i.e. rejecting suspected or other complications, we estimate an average risk of approximately 0.35% of pregnancies experiencing ZIKV infection. Including the 3

foetal deaths where ZIKV infections were confirmed during pregnancy, i.e. using a total of 24 cases, only increased the risk to 0.39%. More generally, based on the results from our fitting approach and using the average birth rates of FSA as guideline, we estimate that on average 3-4 MC cases are expected per 100k individuals at 65% exposure to the virus.

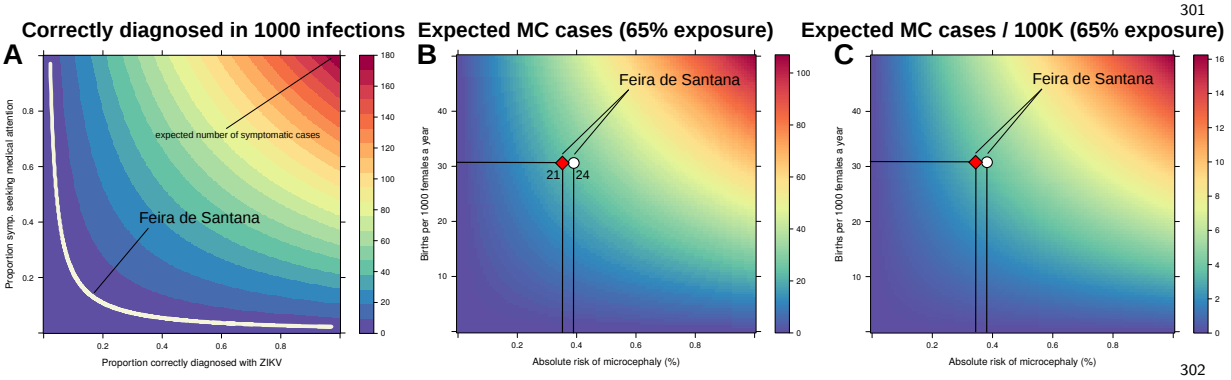

Figure 5 - Sensitivity to reporting and microcephaly risk in Feira de Santana (FSA). *(A)* The observation rate (OR) can be expressed as the product of the proportion of cases that are symptomatic (0.18 [44]), with the proportion of symptomatic that seek medical attention, and the proportion of symptomatic that upon medical attention get correctly diagnosed with Zika. In the white area the expected number of notified cases is the range obtained from fitting FSA case data (OR=0.0039, 95% CI [0.0038-0.0041], Figure 3). *(B)* Expected number of cases of microcephaly (MC) for theoretical ranges of birth rate (per 1,000 females) and risk of MC assuming 65% exposure of all pregnancies as estimated by our model for 2015 in FSA. *(C)* Expected number of MC per 100,000 individuals under the same conditions as in *B*. The symbols in *B* and C represent the total confirmed MC cases (21, red diamond), and the 21 MC plus 3 fetal deaths with confirmed Zika infection (24, white circle); the dashed horizontal line marks the number of births for FSA in 2015, and the vertical lines are the estimated risks per pregnancy.

Discussion

Using an ento-epidemiological transmission model, driven by temporal climate data and fitted to notified case data, we analysed the 2015-2017 Zika outbreak in the city of Feira de Santana (FSA), in the Bahia state of Brazil and determined the conditions that led to the rapid spread of the virus as well as its future endemic and epidemic potential in this region. Given FSA's high suitability for ZIKV mosquito-vectors and its particular geographical setting as a state commerce and transport hub, our results should have major implications for other urban centres in Brazil and elsewhere.

The pattern of reported ZIKV infections in FSA was characterized by a large epidemic in 2015, in clear contrast to total reports at the country-level, peaking during 2016. Most notably for FSA was the epidemic decay in 2016 and fadeout in 2017. In order to resolve whether this was due to a lower transmission potential of ZIKV in 2016/2017 in FSA,

we calculated the daily reproductive number (R_0) between 2013 and 2017 but found no notable decrease in 2016. Interestingly, the maximum R_0 in that period was observed in the season 2015/2016, coinciding with El Niño [49] and thus in line with the hypothesis that this phenomenon may temporary boost arboviral potential [50, 31]. By fitting our model to weekly case data we also estimated the observation rate, i.e. the fraction of cases that were notified as Zika out of the estimated total number of infections. It has previously been reported that the vast majority of Zika infections go unnoticed (Table 1), which is in agreement with our estimates of an observation rate below 1%. Based on this, around 65% of the local population were predicted to have been infected by ZIKV during the first wave in 2015, which is in the same range as the reported Zika outbreaks in French Polynesia (66%) [46] and Yap Island (73%) [44]. The accumulation of herd-immunity caused a substantial drop in the virus's effective reproductive number (R_e) and hence a significantly lower number of cases during the second wave in 2016 and subsequent demise in 2017. In the context of FSA, it is possible that the high similarity of case definition to DENV, the concurrent CHIKV epidemic, and the low awareness of ZIKV at that time could have resulted in a significant number of ZIKV infections being classified as either dengue or chikungunya. Furthermore, based on our analysis, we would argue that the percentage of correctly diagnosed ZIKV infections and infected individuals seeking medical attention must have been exceptionally low (both lower than 20%).

The age structure of notified cases showed a higher than expected incidence risk ratio (IRR) for individuals under the age of 4 years and a lower than expected risk for individuals aged +50 years. This contrasts the observation during the Zika outbreak on Yap Island in 2007, where all age classes, except the elderly, presented similar attack rates [44]. We note here, however, that the Yap Island analysis was based on both a retrospective analysis of historical hospital records and prospective surveillance (serology, surveys). It is therefore possible that the signatures amongst the youngest and oldest individuals in FSA may reflect deficiencies and / or biases in local notified data. Such signatures could emerge by both a rush of parents seeking medical services driven by a hyped media coverage or prioritization of child-care due to the emergence of microcephaly during the Zika epidemic and a small proportion of the elderly seeking or having access to medical attention. In fact, the increased risk in young children in 2016 may have been a result of increased awareness as well as the interventions by the WHO in the second year. We also found a small increase in IRR in the 20-34 years age group, particularly during 2016, which could be indicative of the small contribution of sexual transmission [26, 24]. Most of these observations are speculative, however, and more detailed data will be required to fully understand these age-related risk patterns. For instance, initiatives such as the ZiBRA Project [51, 36, 52], which perform mobile and real-time sampling with portable genome sequencing, could prove to be essential for a retrospective and future analysis of the ZIKV epidemic in Brazil, especially in areas where high levels of herd-immunity will prevent large-scale circulation in the coming years [17].

The implicit consideration of climate variables as drivers of vector biology allowed us to ascertain the relative roles of temperature, humidity and rainfall for Zika's basic and effective reproductive potentials (R_0 and R_e, respectively). Similar to other studies in temperate and tropical settings, we found that temperature, with its direct influence on mosquito lifespan, aquatic development and extrinsic incubation period, was the key driver of seasonal

oscillations in the transmission potential [28, 53, 33, 29]. Rainfall, on the other hand, only seemed to play a marginal role and we argue that it may be a relevant player for arboviral transmission mainly in tropical regions subject to intense rain seasons, such as areas in South East Asia [54, 55, 56]. We also noted that the correlations between climatic variables and case counts were inverted when addressed against the transmission potential. For instance, while temperature was positively correlated with R_0 it was negatively correlated with Zika cases. This implies that the transmission potential is readily responsive to climatic variation but that the Zika epidemics in FSA showed a slight but expected delay in relation to the peak in transmission potential, with case numbers generally increasing after a stable period of maximum R_0, followed by epidemic peaks that tended to coincide with declining R_0. An interesting observation is that the 2015 epidemic peaked approximately 3 months after the estimated peak in the virus's transmission potential, whereas there was much higher synchrony during the second wave in 2016. The same behaviour has been described for the CHIKV outbreak in FSA in 2014-2015 and which has been linked to highly discordant spatial distributions between the first two epidemics [5]. It is likely that similar spatial effects [57] were present in FSA's ZIKV outbreaks. Unfortunately we did not have access to sufficiently detailed spatial data to explore this hypothesis further.

A phylogenetic analysis has proposed that the introduction of ZIKV into Bahia took place between March and September 2014, although without direct evidence for its circulation in FSA at that time [58]. Our estimated date of introduction showed support for a date in early-mid December 2014, a few months after the proposed introduction into Bahia and just over 7 weeks before the first case of Zika was notified in FSA. Similar periods between the first notification and estimated introduction often represent the time taken to complete one or more full transmission cycles (human-mosquito-human) before a cluster of cases is generated of sufficient size for detection by passive surveillance systems [28]. The case data also shows a 2-months period after the first notification during which weekly case numbers remained extremely low. This long period was unexpected as persistent circulation of ZIKV could hardly be justified by the observed total of only 10 cases. Given our estimated observation rate, however, the number of ZIKV infections during this time could have amounted to over 2,700 actual cases. In April, the number of cases increased rapidly, coinciding with the Micareta festival, which we argue may have played a role in igniting the exponential phase of the epidemic by facilitating human-vector mixing as well as a more rapid geographical expansion.

After calibrating our model to the 2015-2017 epidemic, we projected the transmission of ZIKV beyond 2017 using stochastic simulations and average climatic variables for this region. Without the possibility of externally acquired infections, local extinction was very likely by 2017 due to the high levels of herd-immunity. According to our study, Zika's reproductive potential (R_e) reached its lowest point in 2017, and it is expected to remain low for the next couple of years, given the slow replenishment of susceptibles in the population through births. When explicitly modelling the importation of infectious cases our projections for the next two decades corroborated the conclusions of previous modelling studies that suggest a weak endemic potential for ZIKV after the initial exhaustion of the susceptible pool [17, 23]. However, our simulations also showed that the future epidemic behaviour is strongly dependent on the frequency of re-introductions, where sporadic and unpredictable epidemics could still be in the order of hundreds of cases. Furthermore, given our estimated

observation rate for the 2015-2017 epidemic, passive surveillance systems are unlikely to fully detect the scale and occurrence of such small epidemics, missing their actual public health impact, and as such efforts should thus be placed to improve ZIKV detection and diagnosis in order to optimize the local reporting rates and potential for control.

Human sexual and vertical transmission of ZIKV is an important public health concern, especially within the context of potential Zika-associated microcephaly (MC) and other neurological complications in pre- and neonatals. With a total of over 10,000 live births in 2015 in FSA, our crude estimate for the risk of Zika-associated MC per pregnancy was below 4 cases per 100,000 individuals in a generalized population under an attack rate of 65%. As discussed elsewhere [46], this risk is extremely low when compared to other known viral-associated complications, such as those caused by infections by cytomegalovirus (CMV) and the rubella virus (RV) [59, 60]. It is therefore crucial to reiterate that what makes the ZIKV a public health concern is not necessarily the per pregnancy risk of neurological complications, but rather the combination of low risk with very high attack rates. Other studies have reported that the risk for complications during the 1^{st} trimester of gestation is higher than the one estimated here. For example, in the French Polynesia (FP) outbreak [46], the risk associated with ZIKV infection during the 1^{st} trimester was 1%, while the overall, full pregnancy risk was 0.42%, similar to our FSA estimates. For the Yap Island epidemic, no microcephaly cases have been reported. With an estimated 24 births per 1,000 females (census 2000 as in [44]) and using an overall risk of approximately 0.4% per pregnancy, only 0-3 cases per 100,000 individuals would have been expected. However, the island's small population size (7391 individuals [44]) together with a general baseline of 0-2 microcephaly cases per 100,000 in many areas of the world [48, 61, 62] would explain the absence of reported cases. It is also important to consider that a variety of birth defects have been found to be statistically associated with Zika virus infection during pregnancy, of which MC is one possible outcome. While the risk for birth defects per pregnancy is consistently reported to be high, estimations for the risk of MC vary considerably. For example, recent clinical trials [9, 10] suggested that the risk of Zika-associated MC could be an order of magnitude higher than the estimate reported in this or other previous studies [46, 44]. At this stage it is not possible to explain these differences, but it is tempting to speculate that other factors must influence either the actual or estimated risk. For example, there could be diagnostic biases or differences between epidemiological and clinical studies. Alternatively, viral or host genetic background, as well as the pre-exposition to other arboviruses may influence the absolute risk experienced by local populations or cohorts.

Official notification of Zika infections in Brazil started on the 1^{st} of January 2016, although cases were reported in many other regions in Brazil during 2015. It is therefore plausible that the observation rate changed upon official guidelines and that the capacity to accurately diagnose and report Zika infections could have been lower in 2015 compared subsequent years. To explore this, we reran our fitting approach allowing for a possible change in the observation rate for 2016 and onwards (Figure 10) and found a similar observation rate for 2015 (0.0039 versus 0.0034) as well as a similar attack rate between the two model variants. However, the estimated observation rate for 2016 and beyond was ≈ 4 times larger than for 2015, implying a positive change due to changes in the surveillance system. Nevertheless, only about 13-14 out of 1000 Zika cases were reported after the 1^{st} of January 2016. It is hard to discern where the positive changes took place, but we suggest

the revised diagnosis guidelines may have increased the proportion correctly diagnosed while the proportion of symptomatic individuals visiting medical facilities did not change. It is also tempting to speculate that the 2015/2016 imbalance in reporting may have been a general phenomenon across Brazil. As described elsewhere, it is thus possible that FSA is a good example of states and urban centres that may have witnessed larger epidemics than reported in 2015 [11]. This, together with our conclusion that low MC risk with very high attack rates makes ZIKV a public health concern, could explain why most MC reports at the level of the country were in 2015 [11], although for many regions the total reported number of ZIKV cases may have been surprisingly small that year.

There are certain limitations to our approach, many of which could be revisited when more detailed data becomes available. For example, we assumed homogeneous mixing between human and mosquito hosts but it is possible that spatio-temporal heterogeneities may have played a role in FSA. Furthermore, we have curated and integrated functional responses of key entomological parameters to temperature, rainfall and humidity variation, which were originally reported for dengue viruses. Our fitting approach is also dependent on notified case data and it is possible that the reported cases are not representative of the initial expansion of the virus, which may have thwarted the obtained posterior of the introduction date. Finally, our future projections for the endemic and epidemic potential of ZIKV are based on average climatic trends of past years and do not capture the occurrence of natural variation between years, in particular for years affected by major Southern American climate events, such as the El Niño [50].

In this study we have addressed the local determinants of ZIKV epidemiology in the context of a major urban centre of Brazil. Our results imply that control and surveillance of ZIKV should be boosted and focused in periods of high temperature and during major social events. These factors could identify windows of opportunity for local interventions to mitigate ZIKV introduction and transmission and should be transferable to other areas for which both temperature data and community event schedules are available. We further confirm that the high transmission potential of ZIKV in urban centres can lead to the exhaustion of the local susceptible pool, which will in turn dictate the long-term epidemic and endemic behaviour of the virus. Depending on the rate of re-introduction, sporadic outbreaks are to be expected, although these will be unlikely to result in a notable increase in the number of microcephaly cases due to their limited sizes and low risk per pregnancy. Nonetheless, these local sporadic occurrences could still have important public health consequences, and we argue that much better diagnostics and reporting rates are required for local authorities to detect and respond to such events in the near future. Our integrated mathematical framework is capable of deriving key insights into the past and future determinants of ZIKV epidemiology and its findings should be applicable to other major urban centres of Brazil and elsewhere.

Materials and Methods

Demographic and socio-economic setting

Feira de Santana (FSA) is a major urban centre of Bahia, located within the state's largest traffic junction, serving as way points to the South, the Southeast and central regions of the country. The city has a population of approximately 620.000 individuals (2015) and serves a greater geographical setting composed of 80 municipalities (*municipios*) summing up to a population of 2.5 million. Although major improvements in water supply have been accomplished in recent decades, with about 90% of the population having direct access to piped water, supply is unstable and is common practice to resort to household storage. Together with an ideal (tropical) local climate, these are favourable breeding conditions for species of the *Aedes* genus of mosquitoes, which are the main transmission vectors of ZIKV, CHIKV and the dengue virus (DENV) that are all co-circulating in the region [30, 37]. FSA's population is generally young, with approximately 30% of individuals under the age of 20 and 60% under the age of 34. In the year of 2015, the female:male sex ratio in FSA was 0.53 and the number of registered births was 10352, leading to a birth rate standard measure of 31 new-borns per 1000 females in the population.

Climate data

Local climatic data (rainfall, humidity, temperature) for the period between January 2013 and May 2017 was collected from the Brazilian open repository for education and research (BDMEP, Banco de Dados Meteorológicos para Ensino e Pesquisa) [63]. The climate in FSA is defined as semi-arid (warm but dry), with sporadic periods of rain concetrated within the months of April and July. Between 2013 and 2015, mean yearly temperature was 24.6 celsius (range 22.5-26.6), total precipitation was 856 mm (range 571-1141), and mean humidity levels 79.5% (range 70.1-88.9%). Temperature, humidity and precipitation per day is available as Dataset 1.

Zika virus notified case data

ZIKV surveillance in Brazil is conducted through the national notifiable diseases information system (Sistema de Informação de Agravos de Notificação, SINAN), which relies on passive case detection. Suspected cases are notified given the presence of pruritic maculopapular rash (flat, red area on the skin that is covered with small bumps) together with two or more symptoms among: low fever, or polyarthralgia (joint pain), or periarticular edema (joint swelling), or conjunctival hyperemia (eye blood vessel dilation) without secretion and pruritus (itching) [64, 65]. The main differences to case definition of DENV and CHIKV are the particular type of pruritic maculopapular rash and low fever (as applied during the Yap Island ZIKV epidemic [44]). The data presented in Figure 1 for both Brazil and FSA represents notified suspected cases and is available as Dataset 3 (please refer to the Acknowledgement section for sources). Here, we use the terms *epidemic wave* and outbreak interchangeably (but see [21]).

Microcephaly and severe neurological complications case data

A total of 53 suspected cases with microcephaly (MC) or other neurological complications were reported in FSA between January 2015 and February 2017. Using guidelines for microcephaly diagnosis provided in March 2016 by the WHO (as in [36]), a total of 21 cases were confirmed after birth and follow-up. A total of 3 fetal deaths were reported for mothers with confirmed ZIKV infection during gestation but for which no microcephaly assessment was available. The first confirmed microcephaly case was reported on the 24^{th} of November 2015 and virtually all subsequent cases were notified before August 2016 (with the exception of 2). The microcephaly case series can be found in Dataset 4.

Ento-Epidemiological Dynamic Model

The ordinary differential equations (ODE) model and the Markov-chain Monte Carlo (MCMC) fitting approach herein used are based on the framework previously proposed to study the introduction of dengue into the Island of Madeira in 2012 [28]. We have changed this framework to relax major modelling assumptions on the mosquito sex ratio and success of egg hatching, have included humidity and rainfall as critical climate variables, and have also transformed the original least squares based MCMC into a Bayesian MCMC. The resulting framework is described in the following sections, in which extra figures are added for completeness.

The dynamics of infection within the human population are defined in equations 1-5. In summary, the human population is assumed to have constant size (N) with mean life-expectancy of μ^h years, and to be fully susceptible before introduction of the virus. Upon challenge with infectious mosquito bites ($\lambda^{v\to h}$), individuals enter the incubation phase (E^h) with mean duration of $1/\gamma^h$ days, later becoming infectious (I^h) for $1/\sigma^h$ days and finally recovering (R^h) with life-long immunity.

$$\frac{dS^h}{dt} = \mu^h N - \lambda^{v\to h} - \mu^h S^h \quad (1)$$

$$\frac{dE^h}{dt} = \lambda^{v\to h} - \gamma^h E^h - \mu^h E^h \quad (2)$$

$$\frac{dI^h}{dt} = \gamma^h E^h - \sigma^h I^h - \mu^h I^h \quad (3)$$

$$\frac{dR^h}{dt} = \sigma^h I^h - \mu^h R^h \quad (4)$$

$$N = S^h + E^h + I^h + R^h \quad (5)$$

For the dynamics of the mosquito population (equations 6-10), individuals are divided into two pertinent life-stages: aquatic (eggs, larvae and pupae, A) and adult females (V) as in [66]. The adults are further divided into the epidemiologically relevant stages for arboviral transmission: susceptible (S^v), incubating (E^v) for $1/\dot{\gamma}^v$ days and infectious (I^v) for life. The $\dot{}$ (dot) notation is here adopted to distinguish climate-dependent entomological factors (further details in the following sections).

$$\frac{dA}{dt} = \dot{c}^v f \dot{\theta}^v \left(1 - \frac{A}{K\,(R+1)}\right) V - (\dot{\epsilon}_A^v + \dot{\mu}_A^v) A \quad (6)$$

$$\frac{dS^v}{dt} = \dot{\epsilon}_A^v A - \lambda^{h\to v} - \dot{\mu}_V^v S^v \quad (7)$$

$$\frac{dE^v}{dt} = \lambda^{h\to v} - \dot{\gamma}^v E^v - \dot{\mu}_V^v E^v \quad (8)$$

$$\frac{dI^v}{dt} = \dot{\gamma}^v E^v - \dot{\mu}_V^v E^v \quad (9)$$

$$V = S^v + E^v + I^v \quad (10)$$

Here, the coefficient $\dot{c}^v$ is the fraction of eggs hatching to larvae and f the resulting female proportion. For simplicity and lack of quantifications for local mosquito populations, it is assumed that the sex ratio remains at 1:1 (i.e. $f = 0.5$). Moreover, $\dot{\epsilon}_A^v$ denotes the rate of transition from aquatic to adult stages, $\dot{\mu}_A^v$ the aquatic mortality, $\dot{\mu}_V^v$ the adult mortality, and $\dot{\theta}^v$ is the success rate of oviposition. The logistic term $(1 - \frac{A}{K(R+1)})$ can be understood as the ecological capacity to receive aquatic individuals [67], scaled by a carrying capacity term $K\,(R+1)$ in which K determines the maximum capacity and R is the local rainfall contribution (further details on following sections).

From equations 6-10, the mean number of viable female offspring produced by one female adult during its life-time, i.e. the basic offspring number Q, was derived (equation 11). Most parameters defining Q are climate-dependent, and for fixed mean values of the climate variables (ex. mean rainfall $\bar{R}$), expressions were derived for the expected population sizes of each mosquito life-stage modelled (A_0, V_0) which are used to initialize the vector population (equations 12-13).

$$Q = \frac{\dot{\epsilon}_A^v}{\dot{\epsilon}_A^v + \dot{\mu}_A^v} \frac{\dot{c} f \dot{\theta}^v}{\dot{\mu}_V^v} \quad (11)$$

$$A_0 = K\,(\bar{R}+1)\left(1 - \frac{1}{Q}\right) \quad (12)$$

$$V_0 = K\,(\bar{R}+1)\left(1 - \frac{1}{Q}\right) \frac{\dot{\epsilon_A^v}}{\dot{\mu_V^v}} \quad (13)$$

Viral Transmission

In respect to the *infected host-type* being considered, the vector-to-human ($\lambda^{v\to h}$) and human-to-vector ($\lambda^{h\to v}$) incidence rates are assumed to be, respectively, density-dependent and frequency-dependent (equations 14-15). Here, $\dot{a^v}$ is the biting rate and $\dot{\phi}^{v\to h}$ and $\phi^{h\to v}$ are the vector-to-human and human-to-vector transmission probabilities per bite. Conceptually, this implies that (i) an increase in the density of infectious vectors should directly raise the risk of infection to a single human, while (ii) an increase in the frequency of infected humans raises the risk of infection to a mosquito biting at a fixed rate. The basic reproductive number (R_0) is defined similarly to previous modelling approaches (equation 16) [68, 69]. We

further derived an expression for the effective reproductive ratio (R_e, equation 17), taking into account the susceptible proportion of the population in real-time.

$$\lambda^{v\to h} = \left(\dot{a^v}\dot{\phi}^{v\to h} I^v S^h/N\right) \propto I^v \quad (14)$$

$$\lambda^{h\to v} = \left(\dot{a^v}\dot{\phi}^{h\to v} I^h S^v/N\right) \propto I^h/N \quad (15)$$

$$R_0 = \frac{(V/N)\ \dot{a^v}\ \dot{a^v}\ \dot{\phi}^{v\to h}\ \phi^{h\to v}\ \dot{\gamma^v}\ \gamma^h}{\dot{\mu}_V^v(\sigma^h+\mu^h)(\gamma^h+\mu^h)(\dot{\gamma^v}+\dot{\mu}_V^v)} \quad (16)$$

$$R_e = (S^h/N)\times(S^v/N)\times R_0/(V/N) \quad (17)$$

Markov Chain Monte Carlo Fitting Approach

For the fitting process, the MCMC algorithm by Lourenco et al. is here altered to a Bayesian approach by formalising a likelihood and parameter priors [28]. For this, the proposal distributions (q) of each parameter were kept as Gaussian (symmetric), effectively retaining a random walk Metropolis kernel. We define our acceptance probability α of a parameter set Θ, given model ODE output y as:

$$\alpha = min\{1, \frac{\pi(y|\Theta^\star)p(\Theta^\star)q(\Theta^o|\Theta^\star)}{\pi(y|\Theta^o)p(\Theta^o)q(\Theta^\star|\Theta^o)}\} \quad (18)$$

where $\Theta^\star$ and Θ^o are the proposed and current (accepted) parameter sets (respectively); $\pi(y|\Theta^\star)$ and $\pi(y|\Theta^o)$ are the likelihoods of the ODE output representing the epidemic data given each parameter set; $p(\Theta^o)$ and $p(\Theta^\star)$ are the prior-related probabilities given each parameter set. We fit the Zika virus cumulative case counts per week, for which no age-related or geographical data is taken into consideration.

For computational reasons and based on a previous approach [70], the likelihoods π were calculated as the product of the conditional Poisson probabilities of each epidemic data (d_i) and ODE (y_i) data point:

$$\pi(y|\Theta) = \prod_{i=1}^{N}[Pr\{y_i = d_i\}] \quad (19)$$

Note, in this case where we have low cases numbers in a large population, the Poisson likelihood represents a reasonable approximation to the Binomial process, which is expected to underlie the observed data.

Fitted Parameters

With the MCMC approach described above, all combinations of the *open* parameters in the ODE system that most likely represent the outbreak are explored (Table 4). In summary, the MCMC estimates the distributions for: (1) the carrying capacity K, an indirect estimate of the number of adult mosquitoes per human; (2) time point of the first case t_0, assumed to be in a human; (3) a linear coefficient η that scales the effect of temperature on aquatic and

adult mortality rates; (4) a linear coefficient α that scales the effect of temperature on the extrinsic incubation period; (5) a non-linear coefficient ρ that scales the effects of humidity and rainfall on entomological parameters; (6) the human infectious period $1/\sigma^h$; and (7) the human incubation period $1/\gamma^h$.

By introducing the linear coefficients η and α, the relative effect of temperature variation on mortality and incubation is not changed *per se*, but instead the baselines are allowed to be different from the laboratory conditions used by Yang *et al.* [66]. For solutions in which $\eta, \alpha \to 1$, the laboratory-based relationships are kept. For a discussion on possible biological factors that may justify η and α please refer to the original description of the method in [28] and [71]. Finally, the introduction of ρ allows the MCMC to vary the strength by which entomological parameters react to deviations from local humidity and rainfall means. In practice, the effect of rainfall and humidity can be switched off when $\rho \to 0$ and made stronger when $\rho \to +\infty$ (details below).

Initial analysis of the MCMC output raised an identifiability issue between the human infectious period ($1/\sigma^h$) and the linear coefficient (η) that scales the effect of temperature on vector mortality (η scales the baseline mortality without changes to the response of mortality to temperature). Hence, changes in both η and $1/\sigma^h$ result in similar scaling effects on the transmission potential R_0 (equation 16) and thus unstable MCMC chains for η and $1/\sigma^h$, with the resulting posteriors appearing to be bimodal (for which there was no biological support). We addressed this issue by using informative priors for four parameters for which biological support exists in the literature: η, $1/\sigma^h$, $1/\gamma^h$, and α. Gaussian priors were used with means and standard deviations taken from the literature (see Figure 7).

Constant Parameters

The framework described above has only 4 fixed parameters that are neither climate-dependent nor estimated in the MCMC approach (Table 3). Amongst these, $\phi^{h\to v}$ is the per bite probability of transmission from human-to-mosquito, which we assume to be 0.5 [72, 73]; the sex ratio of the adult mosquito population f is assumed to be 1:1 [72, 73]; the life-expectancy of the human population is assumed to be an average of 75 years [74]; and the biting rate is taken to be on average 0.25 although with the potential to vary dependent on humidity levels (details below) [41, 75].

Climate-Dependent Parameters

For each of the temperature-dependent entomological parameters, polynomial expressions are found *de novo* or taken from previous studies fitting laboratory entomological data with temperature (T) values used in Celsius. For rainfall (R) and humidity (U), positive or negative relationships to entomological parameters are introduced using simple expressions, with values used after normalization to $[0, 1]$. We assume that some parameters are affected by a combination of temperature with either rainfal or humidity, but take their effects to be independent. A list of climate-dependent parameters and references is found in Table 2.

Polynomials of 4th degree for the mortality (μ_A^v, μ_V^v) and success ovipositon (θ^v) rates

are taken from the study by Yang and colleagues under temperature-controlled experiments on populations of *Aedes aegypti* (equations 19-21) [66]. For aquatic to adult (ϵ_A^v) rate we use the 7^{th} degree polynomial of the same study (equation 20). For the relationship between the extrinsic incubation period ($1/\gamma^v$) and temperature we apply the formulation by Focks et al. which assumes that replication is determined by a single rate-controlling enzyme [76, 77, 78] (equation 24). The probability of transmission per mosquito bite ($\phi^{v\to h}$) is here modelled (equation 25) as estimated by Lambrechts and colleagues [79]. Finally, the relationship between temperature and the fraction of eggs that successfully hatch (c^v) is estimated *de novo* (equation 26) by fitting a 3^{rd} degree polynomial to *Aedes aegypti* and *albopictus* empirical data described by Dickerson et al. (see Figure 6) [80, 73].

$$\begin{aligned}
\epsilon_A^v(T) &= 0.131 - 0.05723T + 0.01164T^2 - 0.001341T^3 + 0.00008723T^4 \\
&\quad -0.0000003017T^5 + 5.153\times10^{-8}T^6 - 3.42\times10^{-10}T^7 && (20)\\
\mu_A^v(T) &= 2.13 - 0.3797T + 0.02457T^2 - 0.0006778T^3 + 0.000006794T^4 && (21)\\
\mu_V^v(T) &= 0.8692 - 0.1599T + 0.01116T^2 - 0.0003408T^3 + 0.000003809T^4 && (22)\\
\theta^v(T) &= -5.4 + 1.8T - 0.2124T^2 + 0.01015T^3 - 0.0001515T^4 && (23)\\
\gamma^v(T) &= \frac{0.003359\frac{Tk}{298}\times\exp(\frac{15000}{R}(\frac{1}{298}-\frac{1}{Tk}))}{1+\exp(\frac{6.203\times10^{21}}{R}(\frac{1}{-2.176\times10^{30}}-\frac{1}{Tk}))} && (24)\\
\phi^{v\to h}(T) &= 0.001044T\times(T-12.286)\times(32.461-T)^{1/2} && (25)\\
c^v(T) &= (-184.8 + 27.94T - 0.9254T^2 + 0.009226T^3)/100.0 && (26)
\end{aligned}$$

We normalise the time series of rainfall (R) and humidity (U), further using the mean normalised values ($\bar{R}, \bar{U}$) as reference for extreme deviations from the expected local tendencies [81, 67]. Rainfall is assumed to affect positively the fraction of eggs that successfully hatch (c^v) [82, 83, 67, 84]. A similar positive relationship is taken for the vector biting rate (a^v) and humidity levels [75], in contrast to a negative effect on the adult mosquito mortality rate (μ_V^v) [82].

$$\begin{aligned}
c^v(R) &= (R-\bar{R})/\sqrt{1+(R-\bar{R})^2} && (27)\\
a^v(U) &= (U-\bar{U})/\sqrt{1+(U-\bar{U})^2} && (28)\\
\mu_V^v(U) &= \bar{U}-(U-\bar{U})/\sqrt{1+(U-\bar{U})^2} && (29)
\end{aligned}$$

Below is the complete formulation for each entomological parameter in time (t), depending on the climatic variables for which relationships are assumed to exist, including the MCMC fitted linear (α, η) and non-linear (ρ) factors described above.

$$\begin{aligned}
\epsilon_A^v(t) &= \epsilon_A^v(T) && (30)\\
\mu_A^v(t) &= \eta\mu_A^v(T) && (31)\\
\mu_V^v(t) &= \eta\mu_V^v(T)[1+\mu_V^v(U)]^\rho && (32)
\end{aligned}$$

$$\theta^v(t) = \theta^v(T) \quad (33)$$
$$\gamma^v(t) = \alpha\gamma^v(T) \quad (34)$$
$$\phi^{v\to h}(t) = \phi^{v\to h}(T) \quad (35)$$
$$c^v(t) = c^v(T)[1 + c^v(R)]^\rho \quad (36)$$
$$a^v(t) = a^v[1 + a^v(U)]^\rho \quad (37)$$

Stochastic formulation of the ento-epidemiological model

A stochastic version of the ento-epidemiological framework was developed by introducing demographic stochasticity in the transitions of the dynamic system. This followed the original strategy described in [28], in which multinomial distributions are used to sample the effective number of individuals transitioning between classes per time step. Multinomial distributions are generalized binomials - $Binomial(n, p)$ - where n equals the number of individuals in each class and p the probability of the transition event (equal to the deterministic transition rate). This approach has also been demonstrated elsewhere [85].

Source code

The approach used in this study uses code in C/C++, bash and R scripts and is available at https://github.com/lourencoj/ArboWeD2/tree/ArboWeD2$_V$1.

Supplementary Files

Dataset 1

Climate time series for Feira de Santana (2013-2017), including daily temperature, humidity and rainfall (FSA_climate_series.xls).

Dataset 2

Age-related data for Feira de Santana (2015), including case counts per age, total population numbers and gender ratios (FSA_age_data.xls).

Dataset 3

Total weekly notified cases in Feira de Santana (2015-2017) (FSA_incidence_series.xls).

Dataset 4

Total notified cases of Microcephaly in Feira de Santana (2015-2017), including confirmed and suspected / not confirmed (FSA_Microcephaly_series.xls).

Supplementary File 1

Sample model deterministic solutions for incidence (Incidence_detsolution.csv).

Supplementary File 2

Sample model deterministic solutions for R0 (R0_detsolution.csv).

Supplementary File 3

Sample model deterministic solutions for Re (Re_detsolution.csv).

Supplementary File 4

Sample model stochastic solutions for incidence (Incidence_stosolution.csv).

Supplementary File 5

Sample model stochastic solutions for R0 (R0_stosolution.csv).

Supplementary File 6

Sample model stochastic solutions for Re (Re_stosolution.csv).

Competing interests

The authors declare no competing interests.

Acknowledgments

We are most grateful to Wanderson Klebeler de Oliveira, Livia Carla Vinhal, Mariana Pastorello Verotti, Giovanini Evelim Coelho and Claudio Maierovitch Pessanha Henrique from the Brazilian Ministry of Health for providing epidemiological data regarding Zika virus notified cases in Brazil.

MML and EMC curated the Zika virus notified cases in Feira de Santana.

JL and ASW received funding from the European Research Council under the European Union's Seventh Framework Programme (FP7/2007-2013) / ERC grant agreement no. 268904 – DIVERSITY. MR was supported by a Royal Society University Research Fellowship. The European Research Council under the European Union's Seventh Framework Program (FP7/2007-2013)/ERC grant agreement no. 614725-PATHPHYLODYN funded OP. MUGK's contribution was made possible by the generous support of the American people through the United States Agency for International Development Emerging Pandemic Threats Program-2 PREDICT-2 (Cooperative Agreement No. AID-OAA-A-14-00102). CJVA was supported by a fellowship from the Labex EpiGenMed, via the National Research Agency, Program for Future Investment and University of Montpellier [ANR-10-LABX-12-01]. BL received funding from the Engineering and Physical Sciences Research Council (EPSRC) in the UK. NRF was supported by a Sir Henry Dale Fellowship jointly funded by the Wellcome Trust and the Royal Society (grant number 204311/Z/16/Z). The funders had no role in study design, data collection and analysis, decision to publish, or preparation of the manuscript.

Tables

Table 1. Literature-based reports on key ZIKV epidemiological and entomological parameters.

Parameter / Function	Values and Ranges Reported	References
Intrinsic incubation period	6.5, 5.9 days	[17, 86]
Human infectious period	4.7, 9.9 days	[17, 86]
Extrinsic incubation period	8.2, <10, <7 days	[17, 87, 88]
Attack rates	74, 50, 73, 94, 52 %	[89, 44, 23, 90]
R_0	3.2, 2.5, 4.8, 2.05, 2.6-4.8, 4.3–5.8, 1.8-2.0	[89, 91, 25, 23, 19]
Observation rate	0.024, 0.06, 0.03, 0.11	[89, 91, 23]

Table 2. Model climate-dependent parameters.

notation	description
$\epsilon_A^v(t)$	transition rate from aquatic to adult mosquito life-stages
$\mu_A^v(t)$	mortality rate of aquatic mosquito life-stage
$\mu_V^v(t)$	mortality rate of adult mosquito life-stage
$\theta^v(t)$	(human) intrinsic oviposition rate of adult mosquito life-stage
$\gamma^v(t)$	(vector) extrinsic incubation period of adult mosquito life-stage
$\phi^{v\to h}(t)$	vector-to-human probability of transmission per infectious bite
$c^v(t)$	egg hatching success
$a^v(t)$	adult vector biting rate

Table 3. Model constant parameters.

notation	value	description	references
a^v	0.25 per day	mosquito biting rate	[41, 75]
f	0.5	proportion of females (sex ratio)	[72, 73]
$\phi^{h\to v}$	0.5	human-to-vector probability of transmission per infectious bite	–
$1/\mu^h$	75 years	human mean lifespan	[74]

Table 4. Model estimated parameters.

notation	description	ranges / priors
t_0	time point of first case (in a human)	(∞, ∞)
K	aquatic carrying capacity	$(0, \infty)$
η	linear factor for mosquito mortality	$(0, \infty)$
α	linear factor for extrinsic incubation period	$(0, \infty)$
ρ	non-linear factor for effects of humidity and rainfall	$(0, \infty)$
σ^h	human infectious period	(0, 15)
γ^h	human (intrinsic) incubation period	(0, 15)
ζ	observation rate	(0, 1)

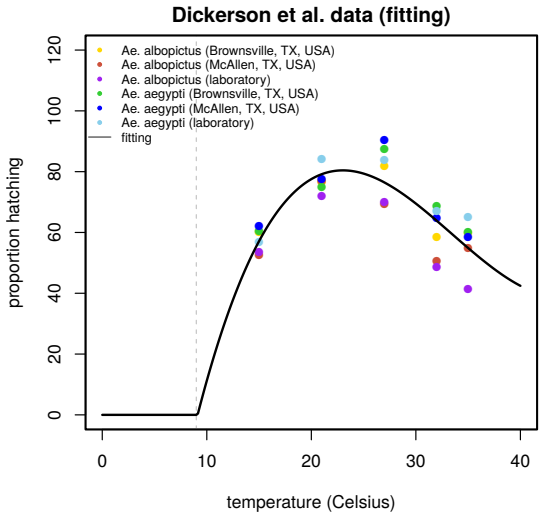

Figure 6 - Relationship between temperature and egg hatching success. Empirical data on *Aedes aegypti's* and *albopictus's* egg hatching success (in the model $\dot{c}$) is taken from [80]. Data includes measurements of hatching for 5 different temperatures above 15 Celsius, including 2 wild and 1 laboratory populations for each of the vector-species. Fitting implemented with a third degree polynomial. When modelling, negative proportions below 10 Celsius are manually corrected to zero (left of shaded grey line).

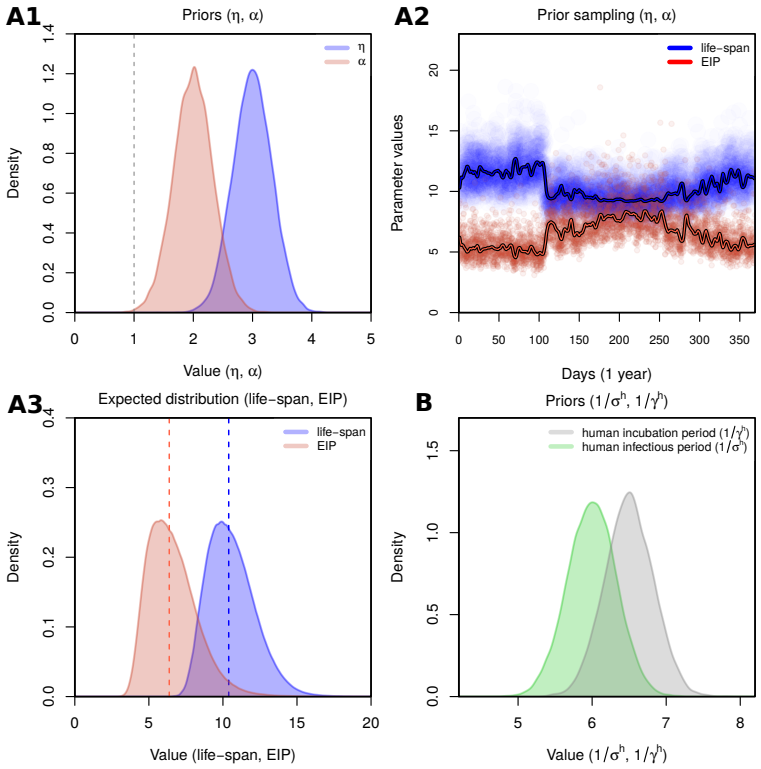

Figure 7 - Prior selection and sensitivity. *(A1)* Priors for the linear coefficients α

(scaling factor for effect of temperature on mosquito incubation period - EIP) and η (scaling factor for effect of temperature on mosquito mortality - life-span). Priors follow Gaussian distributions: α with $mean = 2.0$ and $SD = 0.33$ (standard deviation); η with $mean = 3.0$ and $SD = 0.33$. Means and SDs are chosen to obtain biologically relevant ranges on the parameters being scaled (see subplots A2-A3). *(A2)* With prior set for each coefficient (η, α) as in A1, temperature values of one year from Feira de Santana are used to demonstrate expected variation in the scaled parameters in time. Lines represent the expected mean per day. *(A3)* Distributions of life-span and EIP for the time period presented in A2. *(A1-A3)* The selected priors derive into life-span and EIP ranges that are biologically relevant for *Aedes* mosquitoes, namely that on average the EIP is assumed to be ≈ 7 days and the life-span just below 2 weeks ([40, 41, 42, 43] and Table 1). It should be noted that the priors have been set to be above 1, as we assume that the effects of climate are stronger outside the ideal laboratory conditions for which mathematical relationships have been formulated (see description of the model). *(B)* Priors for the human incubation and infectious period. Means and SDs based on previous estimations [17]. *(A1-A3, B)* Distributions are drawn using 20,000 samples. Representative samples of 500 MCMC chain states are available in Supplementary Files 1-6.

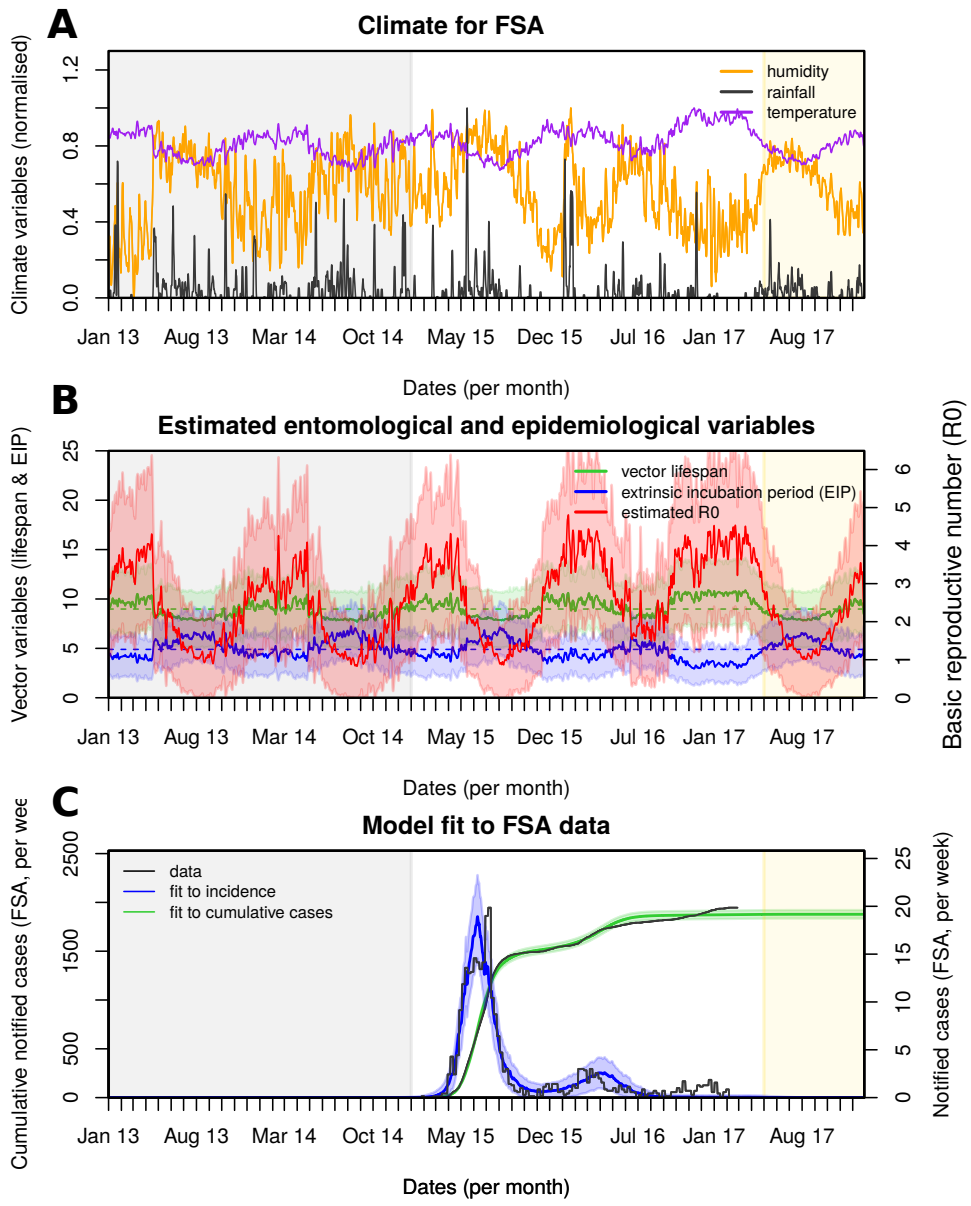

Figure 8 - Eco-epidemiological factors and model fit to notified cases. *(A)* Daily climatic series for rainfall (black), humidity (orange) and mean temperature (purple) for Feira de Santana (FSA). *(B)* Estimated vector lifespan (green), extrinsic incubation period (EIP, blue) and basic reproduction number (R_0, red). Median values are represented by horizontal dashed lines, with around 9 days for the mosquito lifespan, 5 days for the EIP and 2.5 for R_0. *(C)* Resulting Bayesian MCMC fit to weekly (black line: data, blue line: model fit) and cumulative incidence (black line: data, green line: model fit). The grey areas highlight the period before the Zika outbreak, the white areas highlight the period for which Zika virus (ZIKV) notified case data was available, and the yellow shaded areas highlight the period for which mean climatic data was used.

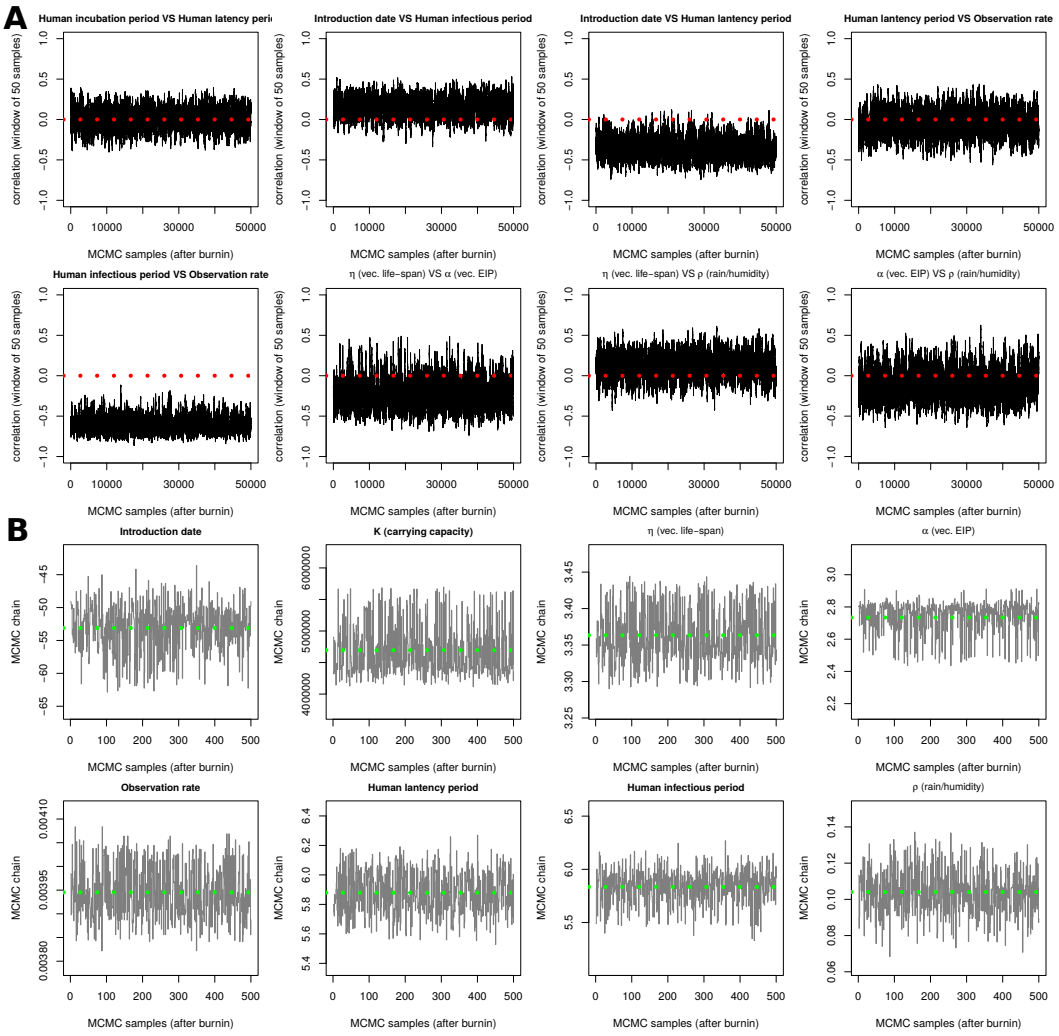

Figure 9 - Sensitivity output for MCMC chains. *(A)* The last 1.5 million states of a 5 million run were sampled (25,000 samples), and the correlation of the states was calculated between the chains of particular parameters (windows of 50 samples for visualization purposes). The correlations present a highly stable behaviour in the MCMC chains. Some parameters, such as the human infectious and latency periods, show no correlation; others show consistently positive or negative correlation. The non-zero correlation is expected between some of the parameters, since fine tuning of certain parameters by the MCMC can be balanced by similar / opposite changes in other parameters, resulting in the same dynamic output; i.e. small identifiability issues are difficult to eliminate from complex ODE models. These correlations may have biological meaning as similar changes in the natural system could follow the relationships herein found. Red dotted lines mark correlation equal to zero. *(B)* MCMC chains for the 8 estimated parameters. The last 1.5 million states of a 5 million run were sampled (1000 samples). The green dotted lines mark the mean. A subsample of 500 was used to run deterministic and stochastic simulations, submitted in spreadsheet tables as supplementary material.

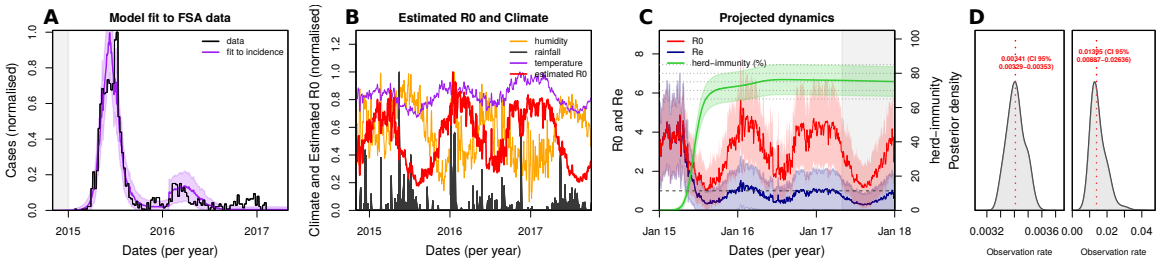

Figure 10 - Eco-epidemiological factors and model fit to notified cases when using 2 observation rates. *(A)* Resulting Bayesian MCMC fit to weekly (black line: data, purple line: model fit) and cumulative incidence (black line: data, grey line: model fit). The grey area highlights the period before the Zika outbreak, the white areas highlight the period for which notified case data was available. *(B)* Climatic series and estimated R_0 for the period of the outbreak (2015-2017), normalised to 1 for visualization purposes (R_0 absolute values in suplot B). *(C)* Fitted and projected epidemic attack rate (% population infected, green), basic reproduction number (R_0, red) and effective reproduction number (R_e, blue). Grey shaded area represents the period after the last available notified case. *(D)* Posteriors for the observation rate of 2015 (left) with median 0.0034 (95% CI [0.0033-0.0035]) and the observation rate for 2016 and onwards (right) with median 0.01395 (95% CI [0.0089-0.0264])).

References

1. Campos G, Bandeira A, Sardi S (2015) Zika Virus Outbreak, Bahia Brazil. Emerging Infectious Diseases 21: 1881.

2. Zanluca C, De Melo VCA, Mosimann ALP, Dos Santos GIV, dos Santos CND, et al. (2015) First report of autochthonous transmission of Zika virus in Brazil. Memorias do Instituto Oswaldo Cruz 110: 569–572.

3. Faria NR, Azevedo RdSdS, Kraemer MUG, Souza R, Cunha MS, et al. (2016) Zika virus in the Americas: Early epidemiological and genetic findings. Science (New York, NY) 352: aaf5036.

4. Nunes MRT, Faria NR, de Vasconcelos JM, Golding N, Kraemer MU, et al. (2015) Emergence and potential for spread of Chikungunya virus in Brazil. BMC Medicine 13: 102.

5. Faria NR, Lourenço J, Marques de Cerqueira E, Maia de Lima M, Carlos Junior Alcantara L (2016) Epidemiology of Chikungunya Virus in Bahia, Brazil, 2014-2015. PLoS Currents .

6. Rubin EJ, Greene MF, Baden LR (2016) Zika Virus and Microcephaly. New England Journal of Medicine 374: 984–985.

7. de Araújo TVB, Rodrigues LC, de Alencar Ximenes RA, de Barros Miranda-Filho D, Montarroyos UR, et al. (2016) Association between Zika virus infection and microcephaly in Brazil, January to May, 2016: Preliminary report of a case-control study. The Lancet Infectious Diseases 16: 1356–1363.

8. Soares de Araújo JS, Regis CT, Gomes RGS, Tavares TR, Rocha Dos Santos C, et al. (2016) Microcephaly in north-east Brazil: a retrospective study on neonates born between 2012 and 2015. Bulletin of the World Health Organization 94: 835–840.

9. Honein MA, Dawson AL, Petersen EE, Jones AM, Lee EH, et al. (2017) Birth Defects Among Fetuses and Infants of US Women With Evidence of Possible Zika Virus Infection During Pregnancy. JAMA 317: 59.

10. Brasil P, Pereira JP, Moreira ME, Nogueira RMR, Damasceno L, et al. (2016) new england journal : 2321–2334.

11. de Oliveira WK, de França GVA, Carmo EH, Duncan BB, de Souza Kuchenbecker R, et al. (2017) Infection-related microcephaly after the 2015 and 2016 Zika virus outbreaks in Brazil: a surveillance-based analysis. The Lancet .

12. WHO WHO Director-General summarizes the outcome of the Emergency Committee regarding clusters of microcephaly and Guillain-Barré syndrome. World Health Organization - Geneva 2016 .

13. WHO Mosquito (vector) control emergency response and preparedness for Zika virus. World Health Organization - Geneva 2016 .

14. Aman MJ, Kashanchi F (2016) Zika virus: A new animal model for an arbovirus. PLoS Neglected Tropical Diseases 10: 1–3.

15. Dowall SD, Graham VA, Rayner E, Atkinson B, Hall G, et al. (2016) A Susceptible Mouse Model for Zika Virus Infection. PLoS Neglected Tropical Diseases 10: 1–13.

16. Chowell G, Hincapie-Palacio D, Ospina J, Pell B, Tariq A, et al. (2016) Using Phenomenological Models to Characterize Transmissibility and Forecast Patterns and Final Burden of Zika Epidemics. PLoS currents 8.

17. Ferguson NM, Cucunubá ZM, Dorigatti I, Nedjati-Gilani GL, Donnelly CA, et al. (2016) Countering the Zika epidemic in Latin America. Science 353: 353–4.

18. Bogoch II, Brady OJ, Kraemer MUG, German M, Creatore MI, et al. (2016) Potential for Zika virus introduction and transmission in resource-limited countries in Africa and the Asia-Pacific region: a modelling study. The Lancet Infectious Diseases 16: 1237–1245.

19. Nishiura H, Kinoshita R, Mizumoto K, Yasuda Y, Nah K (2016) Transmission potential of Zika virus infection in the South Pacific. International Journal of Infectious Diseases 45: 95–97.

20. Zhang Q, Sun K, Chinazzi M, Pastore-Piontti A, Dean NE, et al. (2016) Projected spread of Zika virus in the Americas. bioRxiv : 066456.

21. Perkins A, Siraj A, Ruktanonchai WC, Kraemer M, Tatem A (2016) Model-based projections of Zika virus infections in childbearing women in the Americas. bioRxiv 1: 039610.

22. Messina JP, Kraemer MUG, Brady OJ, Pigott DM, Shearer FM, et al. (2016) Mapping global environmental suitability for Zika virus. eLife 5: 1–19.

23. Kucharski AJ, Funk S, Eggo RM, Mallet HP, Edmunds WJ, et al. (2016) Transmission Dynamics of Zika Virus in Island Populations: A Modelling Analysis of the 2013–14 French Polynesia Outbreak. PLoS Neglected Tropical Diseases 10: 1–15.

24. Maxian O, Neufeld A, Talis EJ, Childs LM, Blackwood JC (2017) Zika virus dynamics: When does sexual transmission matter? Epidemics .

25. Gao D, Lou Y, He D, Porco TC, Kuang Y, et al. (2016) Prevention and Control of Zika as a Mosquito-Borne and Sexually Transmitted Disease: A Mathematical Modeling Analysis. Scientific Reports 6: 28070.

26. Moghadas SM, Shoukat A, Espindola AL, Pereira RS, Abdirizak F, et al. (2017) Asymptomatic Transmission and the Dynamics of Zika Infection. Scientific Reports 7: 5829.

27. Bewick S, Fagan WF, Calabrese JM, Agusto F (2016) Zika Virus: Endemic Versus Epidemic Dynamics and Implications for Disease Spread in the Americas. bioRxiv : 041897.

28. Lourenço J, Recker M (2014) The 2012 Madeira dengue outbreak: epidemiological determinants and future epidemic potential. PLoS neglected tropical diseases 8: e3083.

29. Feldstein LR, Brownstein JS, Brady OJ, Hay SI, Johansson MA (2015) Dengue on islands: a Bayesian approach to understanding the global ecology of dengue viruses. Transactions of the Royal Society of Tropical Medicine and Hygiene 109: 303–12.

30. Kraemer MUG, Sinka ME, Duda KA, Mylne AQN, Shearer FM, et al. (2015) The global distribution of the arbovirus vectors Aedes aegypti and Ae. Albopictus. eLife 4: 1–18.

31. van Panhuis WG, Choisy M, Xiong X, Chok NS, Akarasewi P, et al. (2015) Region-wide synchrony and traveling waves of dengue across eight countries in Southeast Asia. Proc Natl Acad Sci U S A 112: 13069–13074.

32. Poletti P, Messeri G, Ajelli M, Vallorani R, Rizzo C, et al. (2011) Transmission potential of chikungunya virus and control measures: The case of italy. PLoS ONE 6.

33. Mourya DT, Yadav P, Mishra AC (2004) Effect of temperature stress on immature stages and susceptibility of Aedes aegypti mosquitoes to chikungunya virus. American Journal of Tropical Medicine and Hygiene 70: 346–350.

34. Salje H, Cauchemez S, Alera MT, Rodriguez-Barraquer I, Thaisomboonsuk B, et al. (2016) Reconstruction of 60 years of chikungunya epidemiology in the philippines demonstrates episodic and focal transmission. Journal of Infectious Diseases 213: 604–610.

35. Yakob L, Kucharski A, Hue S, Edmunds WJ (2016) Low risk of a sexually-transmitted Zika virus outbreak. The Lancet Infectious Diseases 16: 1100–1102.

36. Faria NR, Sabino EC, Nunes MRT, Alcantara LCJ, Loman NJ, et al. (2016) Mobile real-time surveillance of Zika virus in Brazil. Genome Medicine 8: 97.

37. Carlson CJ, Dougherty ER, Getz W (2016) An Ecological Assessment of the Pandemic Threat of Zika Virus. PLoS Neglected Tropical Diseases 10: 1–18.

38. Foy BD, Kobylinski KC, Foy JLC, Blitvich BJ, da Rosa AT, et al. (2011) Probable Non-Vector-borne Transmission of Zika Virus, Colorado, USA. Emerging Infectious Diseases 17: 880–882.

39. Turmel JM, Abgueguen P, Hubert B, Vandamme YM, Maquart M, et al. (2016) Late sexual transmission of Zika virus related to persistence in the semen. The Lancet 387: 2501.

40. Trpis M, Hausermann W (1995) Population Size, Dispersal, and Longevity of Domestic Aedes aegypti aegypti (Diptera: Culicidae) by Mark-Release-Recapture in the Village of Shauri Moyo in Eastern. Journal of medical 32: 27–33(7).

41. Trpis M, Hausermann W (1986) Dispersal and other population parameters of Aedes aegypti in an African village and their possible significance in epidemiology of vector-borne diseases. American Journal of Tropical Medicine and Hygiene 35: 1263.

42. Andraud M, Hens N, Marais C, Beutels P (2012) Dynamic epidemiological models for dengue transmission: a systematic review of structural approaches. PloS ONE 7: e49085.

43. Hugo LE, Jeffery JAL, Trewin BJ, Wockner LF, Thi Yen N, et al. (2014) Adult Survivorship of the Dengue Mosquito Aedes aegypti Varies Seasonally in Central Vietnam. PLoS Neglected Tropical Diseases 8.

44. Duffy MR, Chen TH, Hancock WT, Powers AM, Kool JL, et al. (2009) Zika Virus Outbreak on Yap Island, Federated States of Micronesia. New England Journal of Medicine 360: 2536–2543.

45. Silva MMO, Rodrigues MS, Paploski IAD, Kikuti M, Kasper AM, et al. (2016) Accuracy of dengue reporting by national surveillance system, Brazil. Emerging Infectious Diseases 22: 336–339.

46. Cauchemez S, Besnard M, Bompard P, Dub T, Guillemette-Artur P, et al. (2016) Association between Zika virus and microcephaly in French Polynesia, 2013-15: A retrospective study. The Lancet 387: 2125–2132.

47. Jaenisch T, Rosenberger K, Brito C, Brady O, Brasil P, et al. (2016) Estimating the risk for microcephaly after Zika virus infection in Brazil. Bulletin of the World Health Organization : 1–15.

48. Johansson MA, Mier-y Teran-Romero L, Reefhuis J, Gilboa SM, Hills SL (2016) Zika and the Risk of Microcephaly. New England Journal of Medicine 375: 1–4.

49. Golden Gate Weather Services. El Niño and La Niña Years and Intensities - Based on Oceanic Niño Index (ONI) - Golden Gate Weather Services. URL `http://ggweather.com/enso/oni.htm`.

50. Caminade C, Turner J, Metelmann S, Hesson JC, Blagrove MSC, et al. (2016) Global risk model for vector-borne transmission of Zika virus reveals the role of El Niño 2015. Proceedings of the National Academy of Sciences 114: 201614303.

51. ZIBRA Zika in Brazil Real Time Analysis Project. Official Webpage .

52. Faria NR, Quick J, Claro I, Thézé J, de Jesus JG, et al. (2017) Establishment and cryptic transmission of Zika virus in Brazil and the Americas. Nature 546: 406–410.

53. Mordecai E, Cohen J, Evans MV, Gudapati P, Johnson LR, et al. (2016) Temperature determines Zika, dengue and chikungunya transmission potential in the Americas. bioRxiv : 63735.

54. Cuong HQ, Hien NT, Duong TN, Phong TV, Cam NN, et al. (2011) Quantifying the Emergence of Dengue in Hanoi, Vietnam: 1998–2009. PLoS Neglected Tropical Diseases 5: e1322.

55. Hii YL, Zhu H, Ng N, Ng LC, Rocklov J (2012) Forecast of dengue incidence using temperature and rainfall. PLoS neglected tropical diseases 6: e1908.

56. Xuan LTT, Van Hau P, Thu DT, Toan DTT (2014) Estimates of meteorological variability in association with dengue cases in a coastal city in northern Vietnam: An ecological study. Global Health Action 7: 1–7.

57. Kraemer MUG, Faria NR, Reiner RC, Golding N, Nikolay B, et al. (2016) Spread of yellow fever virus outbreak in Angola and the Democratic Republic of the Congo 2015–16: a modelling study. The Lancet Infectious Diseases 3099: 1–9.

58. Naccache SN, Thézé J, Sardi SI, Somasekar S, Greninger AL, et al. (2016) Distinct Zika Virus Lineage in Salvador, Bahia, Brazil. Emerging Infectious Diseases 22: 1788–1792.

59. De Santis M, Cavaliere AF, Straface G, Caruso A (2006) Rubella infection in pregnancy. Reproductive toxicology (Elmsford, NY) 21: 390–8.

60. Naing ZW, Scott GM, Shand A, Hamilton ST, van Zuylen WJ, et al. (2016) Congenital cytomegalovirus infection in pregnancy: a review of prevalence, clinical features, diagnosis and prevention. The Australian & New Zealand journal of obstetrics & gynaecology 56: 9–18.

61. Butler D (2016) Zika virus: Brazil's surge in small-headed babies questioned by report. Nature 530: 13–4.

62. EUROCAT (2003) European surveillance of congenital anomalies, final activity report 2002–2003. (http://eceuropaeu/health/ ph_threats/non_com/docs/eurocat_enpdf) .

63. Brazil BDMEP. Banco de Dados Meteorológicos para Ensino e Pesquisa .

64. Brazil SINAN. Sistema de Informação de Agravos de Notificação (national notifiable diseases information system) .

65. Brazil ZIKV Guidelines. National guidelines for Zika virus pathology and diagnosis (2016) .

66. Yang HM, Macoris MLG, Galvani KC, Andrighetti MTM, Wanderley DMV (2009) Assessing the effects of temperature on the population of Aedes aegypti, the vector of dengue. Epidemiology and infection 137: 1188–202.

67. Tran A, L'Ambert G, Lacour G, Benoît R, Demarchi M, et al. (2013) A rainfall- and temperature-driven abundance model for Aedes albopictus populations. International Journal of Environmental Research and Public Health 10: 1698–1719.

68. Wearing HJ, Rohani P (2006) Ecological and immunological determinants of dengue epidemics. Proceedings of the National Academy of Sciences of the United States of America 103: 11802–11807.

69. Lourenço J, Recker M (2013) Natural, persistent oscillations in a spatial multi-strain disease system with application to dengue. PLoS Computational Biology 9: e1003308.

70. Dorigatti I, Cauchemez S, Ferguson NM (2013) Increased transmissibility explains the third wave of infection by the 2009 H1N1 pandemic virus in England. Proceedings of the National Academy of Sciences of the United States of America 110: 13422–13427.

71. Brady OJ, Johansson MA, Guerra CA, Bhatt S, Golding N, et al. (2013) Modelling adult Aedes aegypti and Aedes albopictus survival at different temperatures in laboratory and field settings. Parasites and vectors 6: 351.

72. Lounibos LP, Escher RL (2008) Sex ratios of mosquitoes from long-term censuses of Florida tree holes. Journal of the American Mosquito Control Association 24: 11–15.

73. Mohammed A, Chadee DD (2011) Effects of different temperature regimens on the development of Aedes aegypti (L.) (Diptera: Culicidae) mosquitoes. Acta tropica 119: 38–43.

74. WHO (2016). World Health Organization - Brazil - Statistics. URL `http://www.who.int/countries/bra/en/`.

75. Yasuno M, Tonn RJ (1960) A study of biting habits of Aedes aegypti in Bangkok, Thailand. Population (English Edition) : 319–325.

76. Focks Da, Daniels E, Haile DG, Keesling JE (1995) A simulation model of the epidemiology of urban dengue fever: literature analysis, model development, preliminary validation, and samples of simulation results. The American journal of tropical medicine and hygiene 53: 489–506.

77. Schoolfield RM, Sharpe PJ, Magnuson CE (1981) Non-linear regression of biological temperature-dependent rate models based on absolute reaction-rate theory. Journal of theoretical biology 88: 719–31.

78. Otero M, Solari HG, Schweigmann N (2006) A stochastic population dynamics model for Aedes aegypti: formulation and application to a city with temperate climate. Bulletin of mathematical biology 68: 1945–1974.

79. Lambrechts L, Paaijmans KP, Fansiri T, Carrington LB, Kramer LD, et al. (2011) Impact of daily temperature fluctuations on dengue virus transmission by Aedes aegypti. Proceedings of the National Academy of Sciences of the United States of America 108: 7460–5.

80. Dickerson CZ (2007) The effects of temperature and humidy on the eggs of Aedes aegypti and Aedes albopictus in Texas. Doctor of philosophy, Texas A and M University.

81. Bicout DJ, Sabatier P (2004) Mapping Rift Valley Fever vectors and prevalence using rainfall variations. Vector borne and zoonotic diseases (Larchmont, NY) 4: 33–42.

82. Alto BW, Juliano SA (2001) Precipitation and temperature effects on populations of Aedes albopictus (Diptera: Culicidae): Implications for range expansion. Journal of Medical Entomology 38: 646–656.

83. Rossi MM, Lopez LF, Massad E (2015) The Dynamics of Temperature- And Rainfall-Dependent Dengue Transmission in Tropical Regions. Annals of Biometrics & Biostatistics 2: 1–6.

84. Madeira NG, Macharelli CA, Carvalho LR (2002) Variation of the oviposition preferences of Aedes aegypti in function of substratum and humidity. Memorias do Instituto Oswaldo Cruz 97: 415–420.

85. Lampoudi S, Gillespie DT, Petzold LR (2009) The multinomial simulation algorithm for discrete stochastic simulation of reaction-diffusion systems. The Journal of chemical physics 130: 094104.

86. Lessler J, Ott CT, Carcelen AC, Konikoff JM, Williamson J, et al. (2016) Times to key events in Zika virus infection and implications for blood donation: A systematic review. Bulletin of the World Health Organization 94: 841–849.

87. Li MI, Wong PSJ, Ng LC, Tan CH (2012) Oral Susceptibility of Singapore Aedes (Stegomyia) aegypti (Linnaeus) to Zika Virus. PLoS Neglected Tropical Diseases 6.

88. Wong PSJ, Li MzI, Chong CS, Ng LC, Tan CH (2013) Aedes (Stegomyia) albopictus (Skuse): A Potential Vector of Zika Virus in Singapore. PLoS Neglected Tropical Diseases 7: 1–5.

89. Champagne C, Salthouse DG, Paul R, Cao-Lormeau VM, Roche B, et al. (2016) Structure in the variability of the basic reproductive number (R0) for Zika epidemics in the Pacific islands. eLife 5.

90. Fagbami AH (1979) Zika virus infections in Nigeria: virological and seroepidemiological investigations in Oyo State. The Journal of hygiene 83: 213–219.

91. Funk S, Kucharski AJ, Camacho A, Eggo RM, Yakob L, et al. (2016) Comparative Analysis of Dengue and Zika Outbreaks Reveals Differences by Setting and Virus. PLoS neglected tropical diseases 10: e0005173.

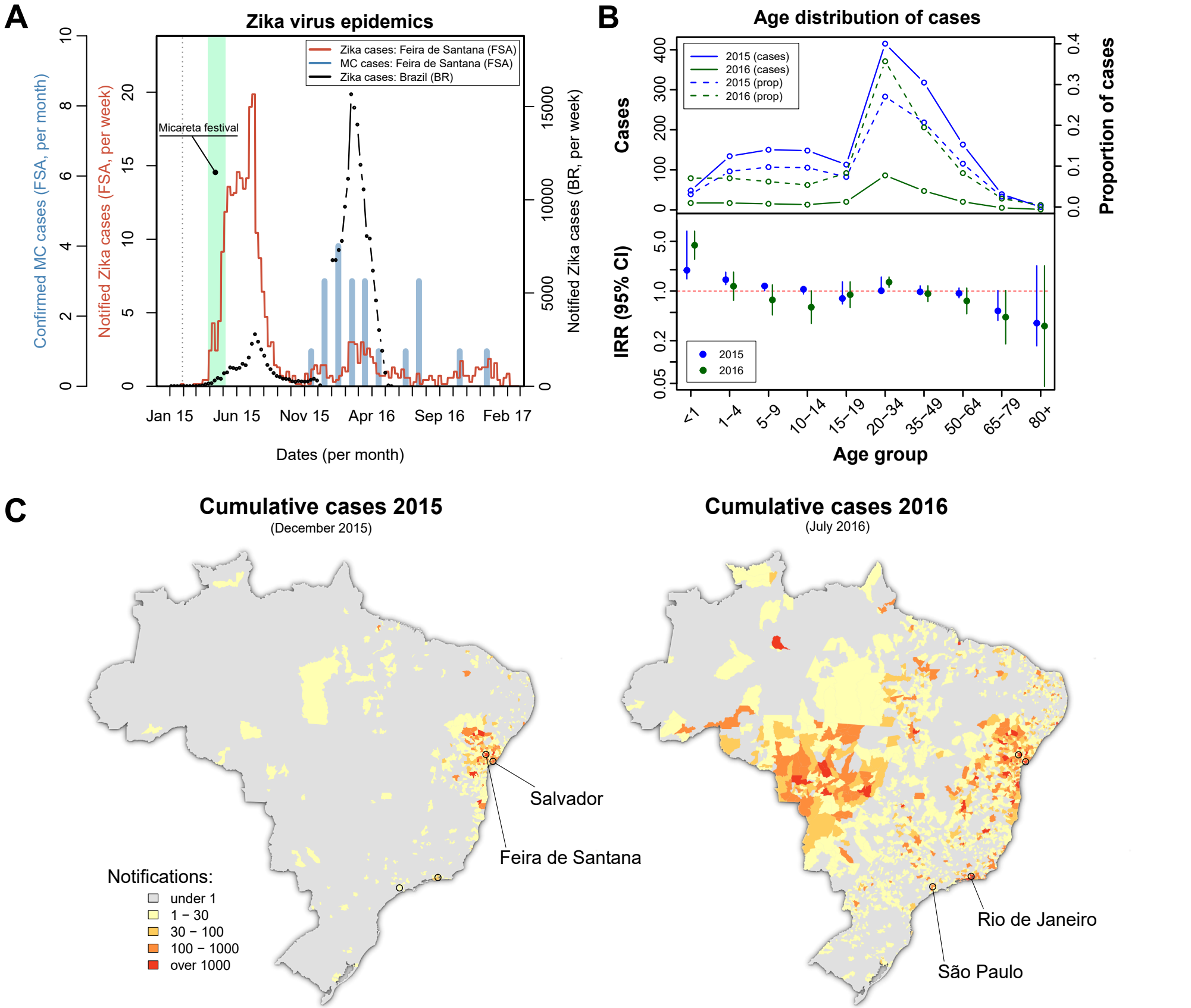
A
Zika virus epidemics
Zika cases: Feira de Santana (FSA)
MC cases: Feira de Santana (FSA)
Zika cases: Brazil (BR)
Micareta festival
Confirmed MC cases (FSA, per month)
Notified Zika cases (FSA, per week)
Notified Zika cases (BR, per week)
Jan 15
Jun 15
Nov 15
Apr 16
Sep 16
Feb 17
Dates (per month)
B
Age distribution of cases
2015 (cases)
2016 (cases)
2015 (prop)
2016 (prop)
Cases
Proportion of cases
IRR (95% CI)
2015
2016
<1
1–4
5–9
10–14
15–19
20–34
35–49
50–64
65–79
80+
Age group
C
Cumulative cases 2015
(December 2015)
Cumulative cases 2016
(July 2016)
Salvador
Feira de Santana
Rio de Janeiro
São Paulo
Notifications:
under 1
1 − 30
30 − 100
100 − 1000
over 1000

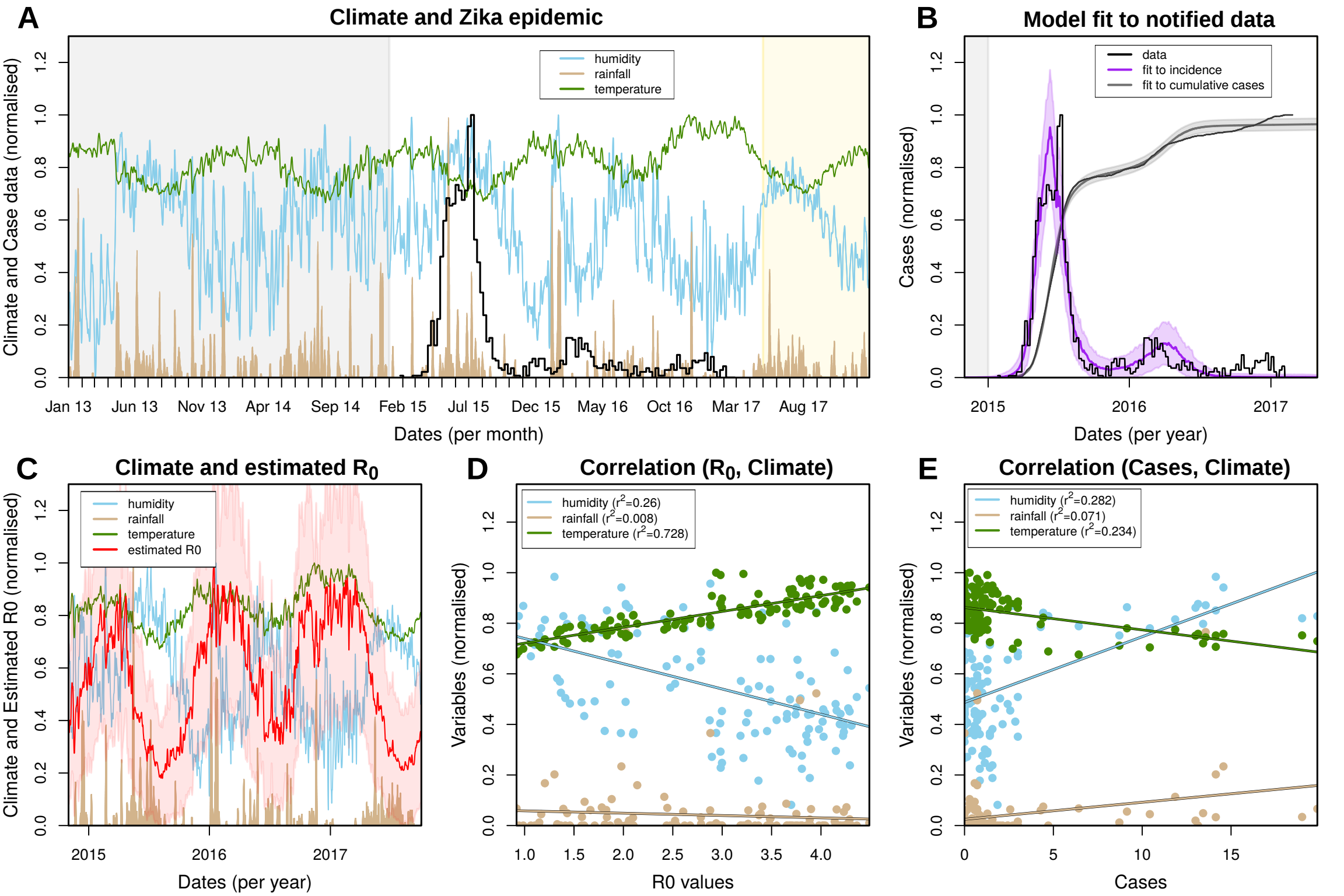
A
Climate and Zika epidemic
humidity
rainfall
temperature
Climate and Case data (normalised)
0.0
0.2
0.4
0.6
0.8
1.0
1.2
Jan 13
Jun 13
Nov 13
Apr 14
Sep 14
Feb 15
Jul 15
Dec 15
May 16
Oct 16
Mar 17
Aug 17
Dates (per month)
B
Model fit to notified data
data
fit to incidence
fit to cumulative cases
Cases (normalised)
2015
2016
2017
Dates (per year)
C
Climate and estimated R0
humidity
rainfall
temperature
estimated R0
Climate and Estimated R0 (normalised)
Dates (per year)
D
Correlation (R0, Climate)
humidity (r2=0.26)
rainfall (r2=0.008)
temperature (r2=0.728)
Variables (normalised)
1.0
1.5
2.0
2.5
3.0
3.5
4.0
R0 values
E
Correlation (Cases, Climate)
humidity (r2=0.282)
rainfall (r2=0.071)
temperature (r2=0.234)
Variables (normalised)
0
5
10
15
Cases

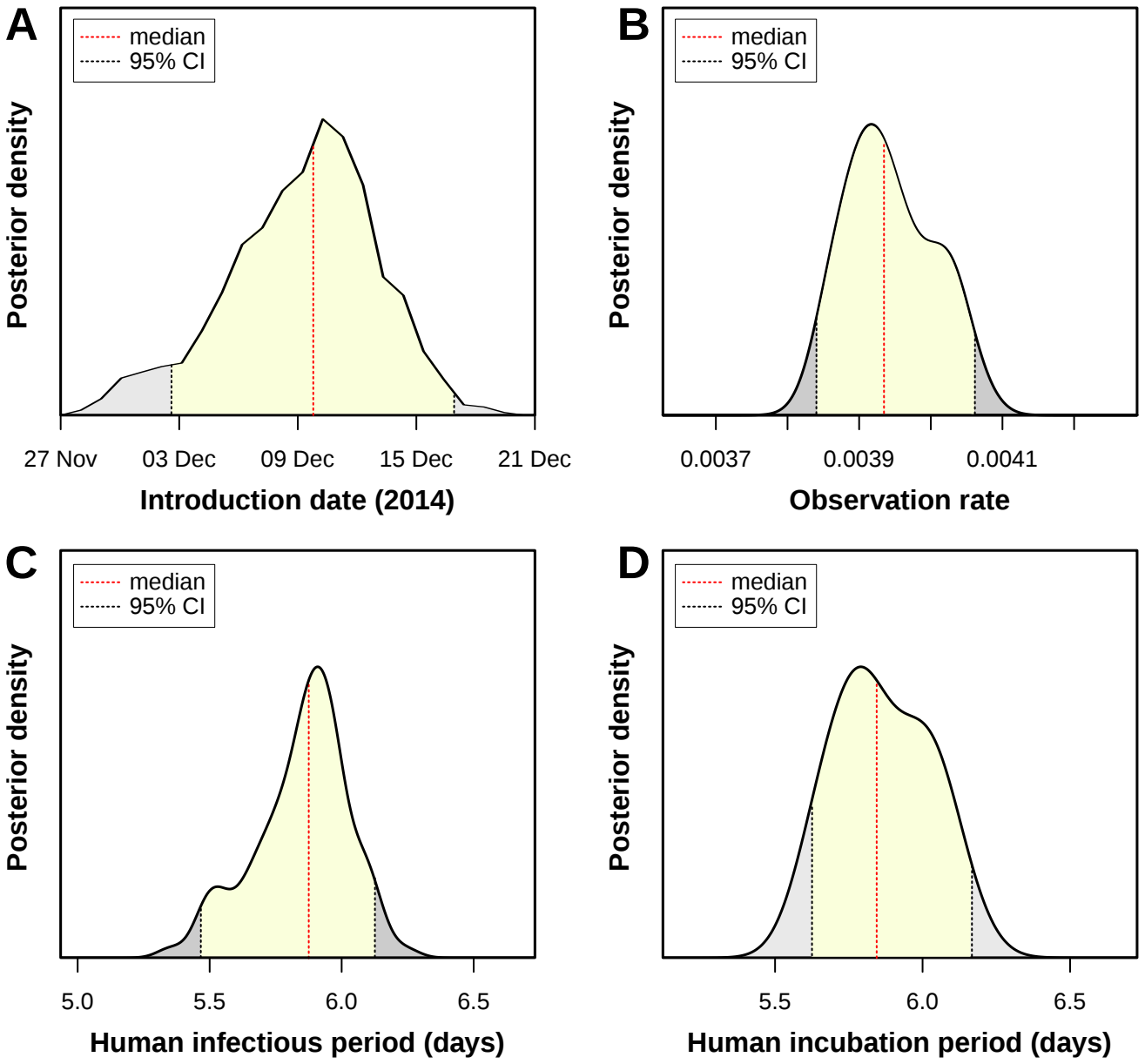
A
median
95% CI
Posterior density
27 Nov
03 Dec
09 Dec
15 Dec
21 Dec
Introduction date (2014)
B
median
95% CI
Posterior density
0.0037
0.0039
0.0041
Observation rate
C
median
95% CI
Posterior density
5.0
5.5
6.0
6.5
Human infectious period (days)
D
median
95% CI
Posterior density
5.5
6.0
6.5
Human incubation period (days)

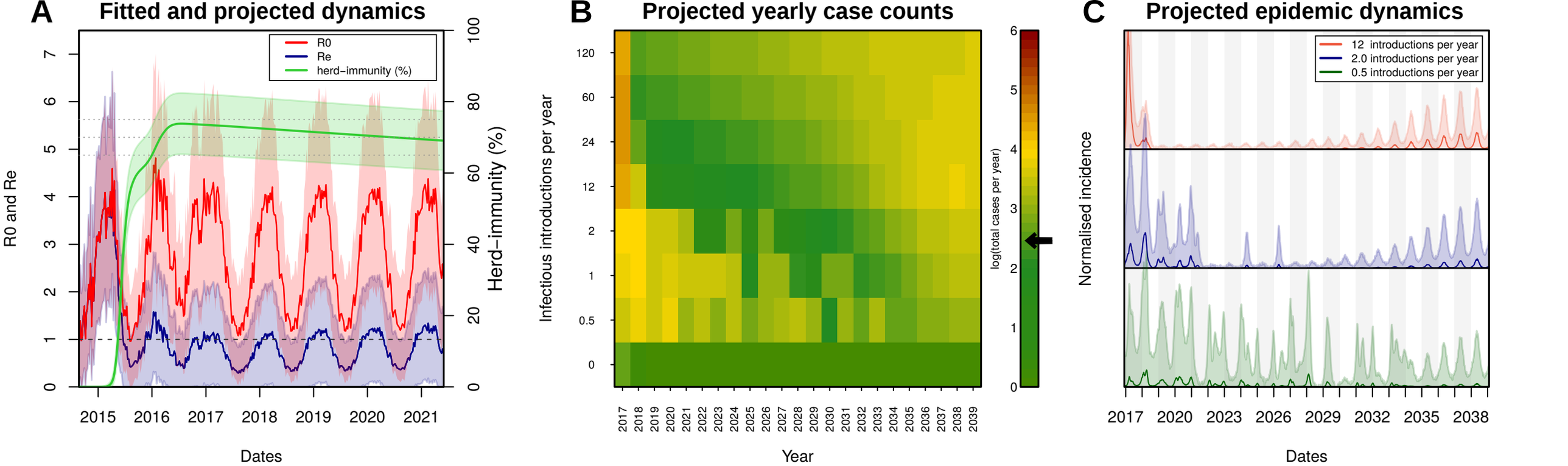
A
Fitted and projected dynamics
R0
Re
herd−immunity (%)
R0 and Re
Herd−immunity (%)
Dates
B
Projected yearly case counts
Infectious introductions per year
Year
log(total cases per year)
C
Projected epidemic dynamics
12 introductions per year
2.0 introductions per year
0.5 introductions per year
Normalised incidence
Dates

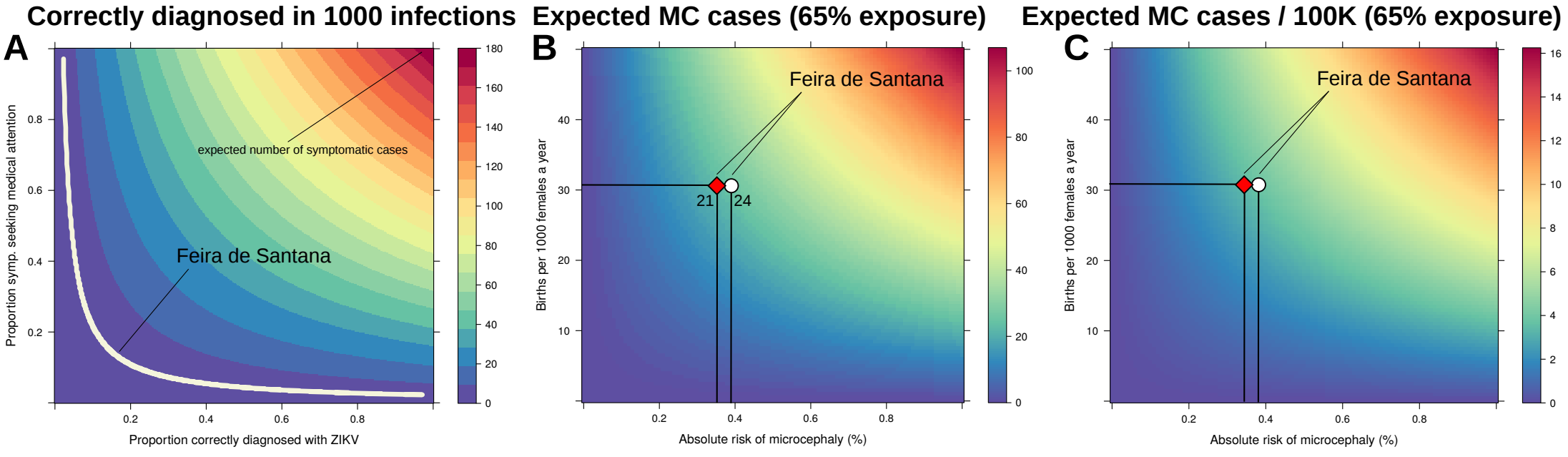
Correctly diagnosed in 1000 infections
Expected MC cases (65% exposure)
Expected MC cases / 100K (65% exposure)
A
B
C
expected number of symptomatic cases
Feira de Santana
Feira de Santana
Feira de Santana
21
24
Proportion symp. seeking medical attention
Proportion correctly diagnosed with ZIKV
Births per 1000 females a year
Absolute risk of microcephaly (%)
Births per 1000 females a year
Absolute risk of microcephaly (%)

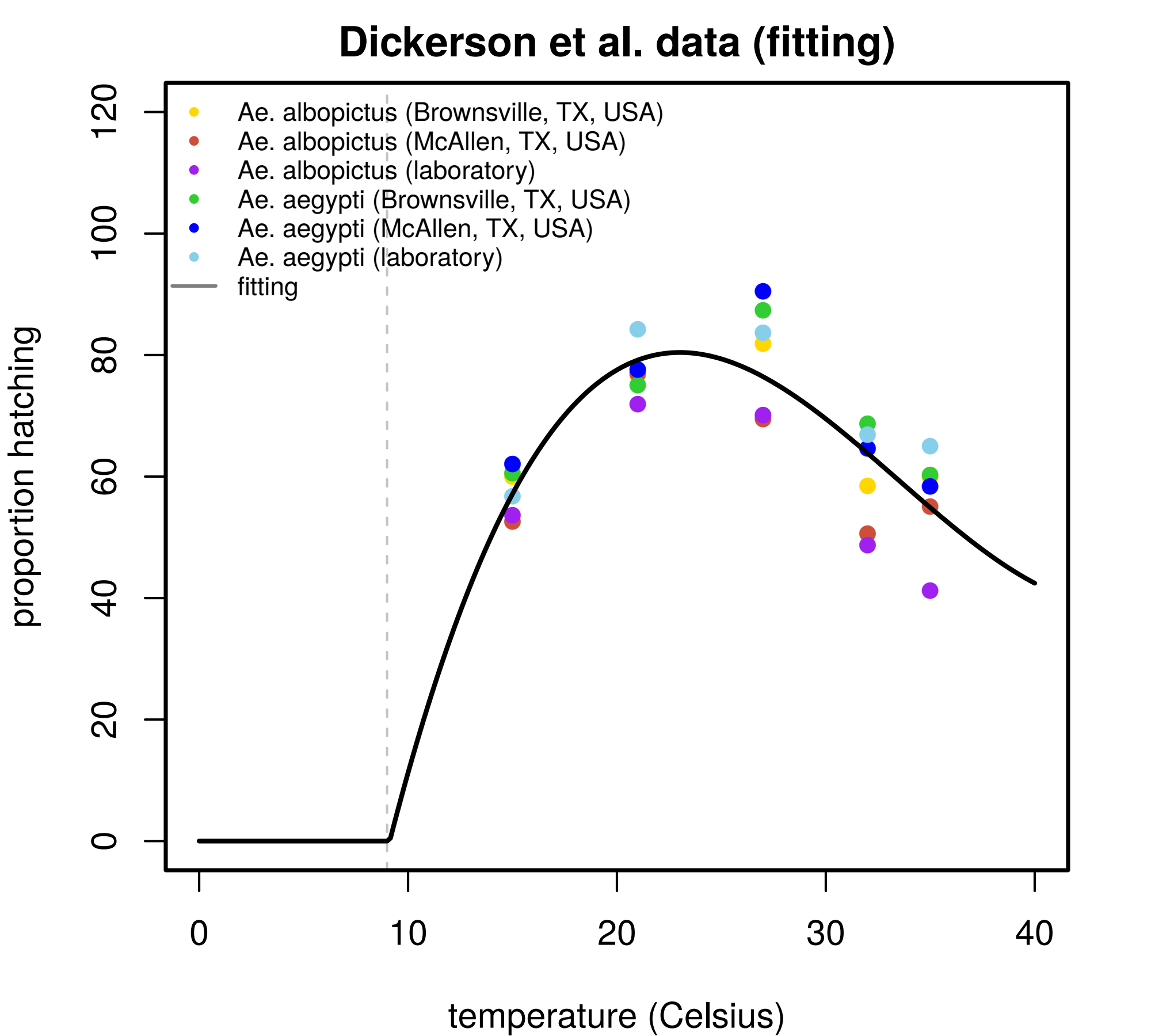
Dickerson et al. data (fitting)
Ae. albopictus (Brownsville, TX, USA)
Ae. albopictus (McAllen, TX, USA)
Ae. albopictus (laboratory)
Ae. aegypti (Brownsville, TX, USA)
Ae. aegypti (McAllen, TX, USA)
Ae. aegypti (laboratory)
fitting
proportion hatching
0
20
40
60
80
100
120
0
10
20
30
40
temperature (Celsius)

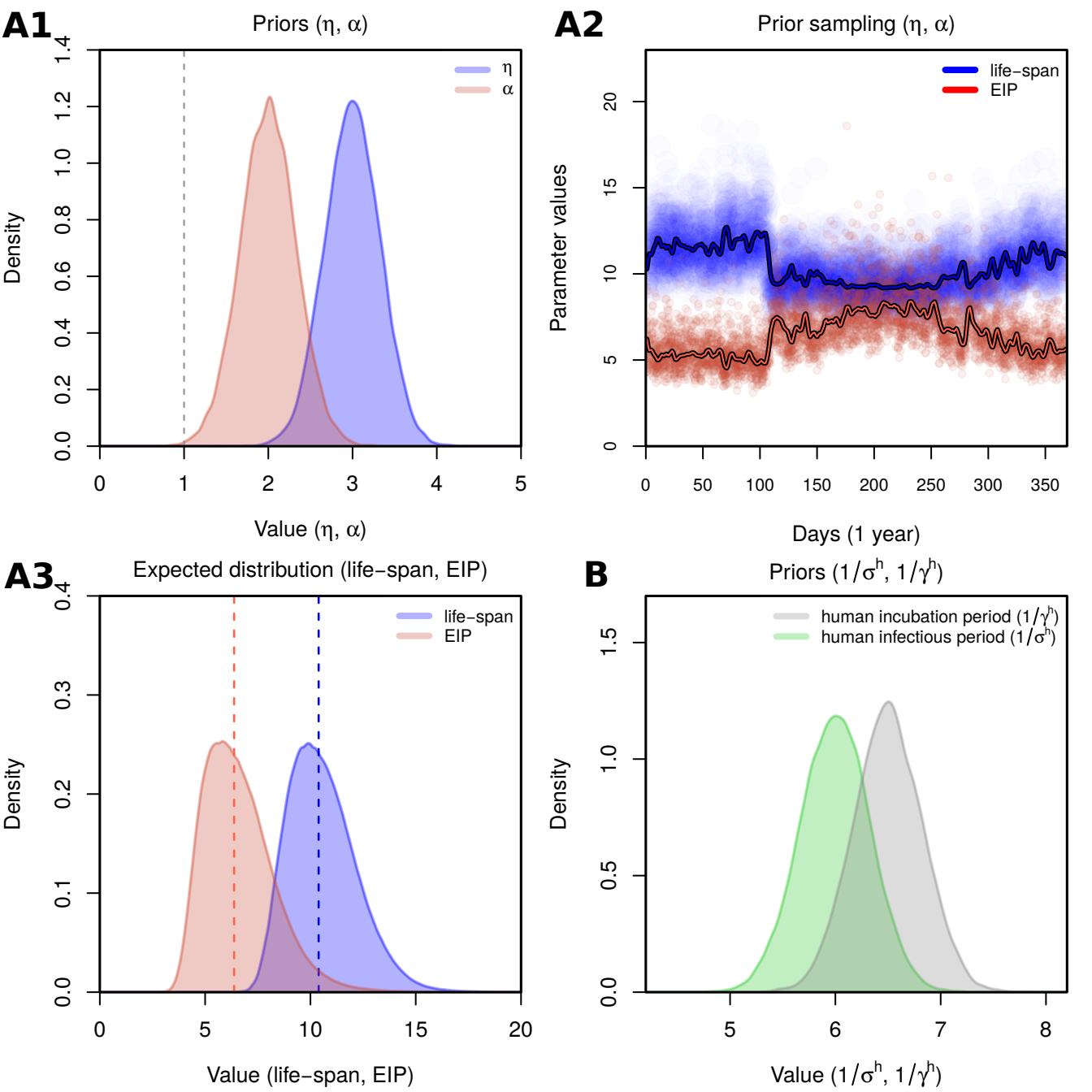
A1
Priors (η, α)
η
α
Density
Value (η, α)
A2
Prior sampling (η, α)
life−span
EIP
Parameter values
Days (1 year)
A3
Expected distribution (life−span, EIP)
life−span
EIP
Density
Value (life−span, EIP)
B
Priors (1/σ^h, 1/γ^h)
human incubation period (1/γ^h)
human infectious period (1/σ^h)
Density
Value (1/σ^h, 1/γ^h)

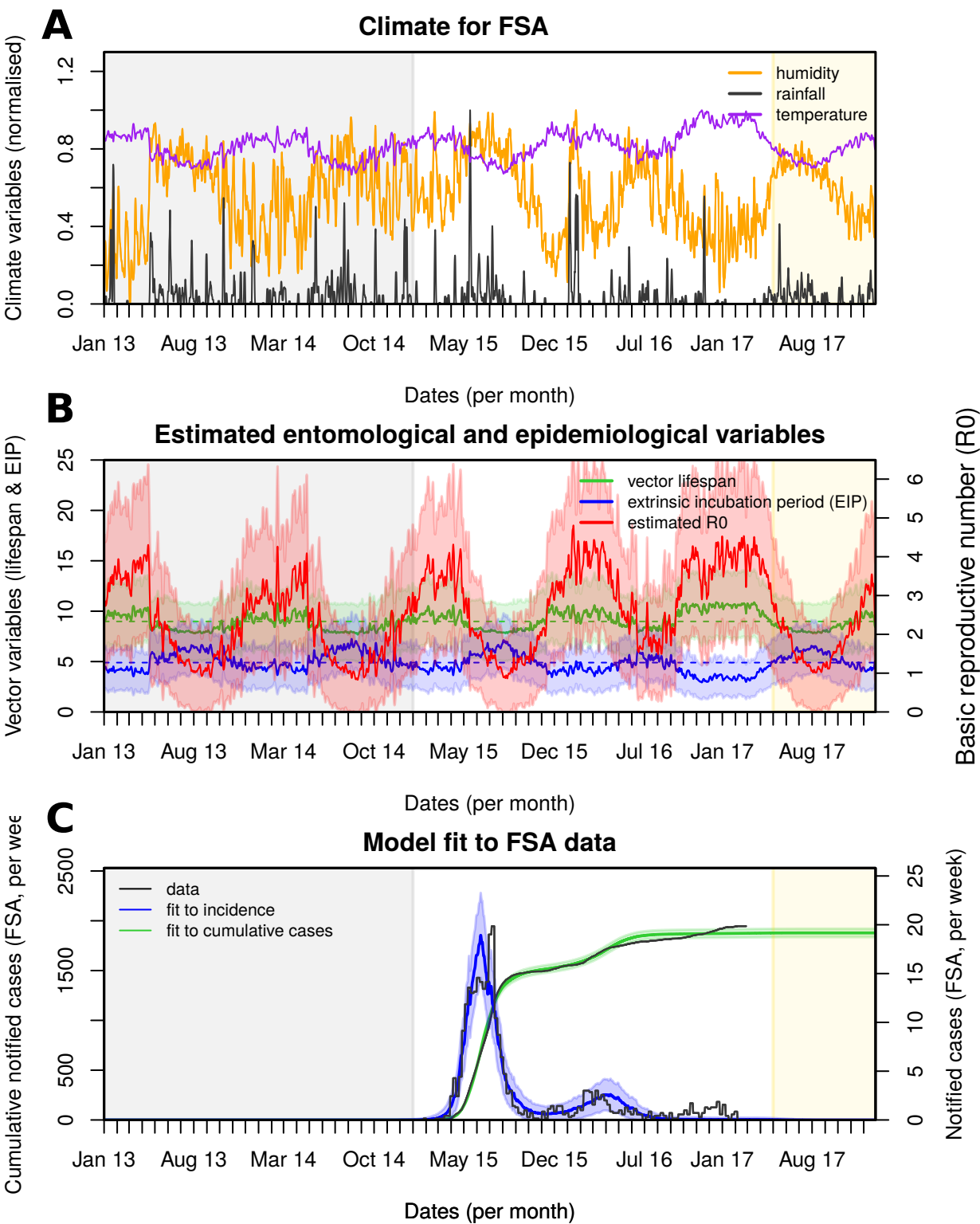
A
Climate for FSA
Climate variables (normalised)
humidity
rainfall
temperature
0.0
0.4
0.8
1.2
Jan 13
Aug 13
Mar 14
Oct 14
May 15
Dec 15
Jul 16
Jan 17
Aug 17
Dates (per month)
B
Estimated entomological and epidemiological variables
Vector variables (lifespan & EIP)
Basic reproductive number (R0)
vector lifespan
extrinsic incubation period (EIP)
estimated R0
0
5
10
15
20
25
0
1
2
3
4
5
6
Jan 13
Aug 13
Mar 14
Oct 14
May 15
Dec 15
Jul 16
Jan 17
Aug 17
Dates (per month)
C
Model fit to FSA data
Cumulative notified cases (FSA, per wee
Notified cases (FSA, per week)
data
fit to incidence
fit to cumulative cases
0
500
1500
2500
0
5
10
15
20
25
Jan 13
Aug 13
Mar 14
Oct 14
May 15
Dec 15
Jul 16
Jan 17
Aug 17
Dates (per month)

A

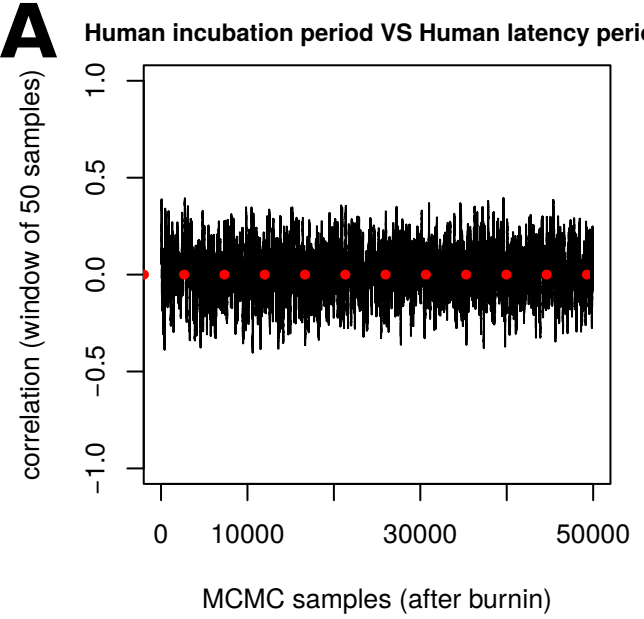
Human incubation period VS Human latency peri
correlation (window of 50 samples)
MCMC samples (after burnin)

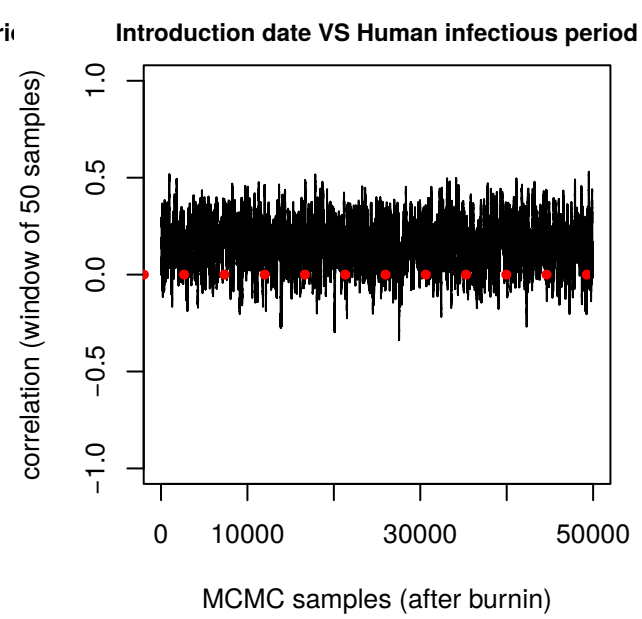
Introduction date VS Human infectious period
correlation (window of 50 samples)
MCMC samples (after burnin)

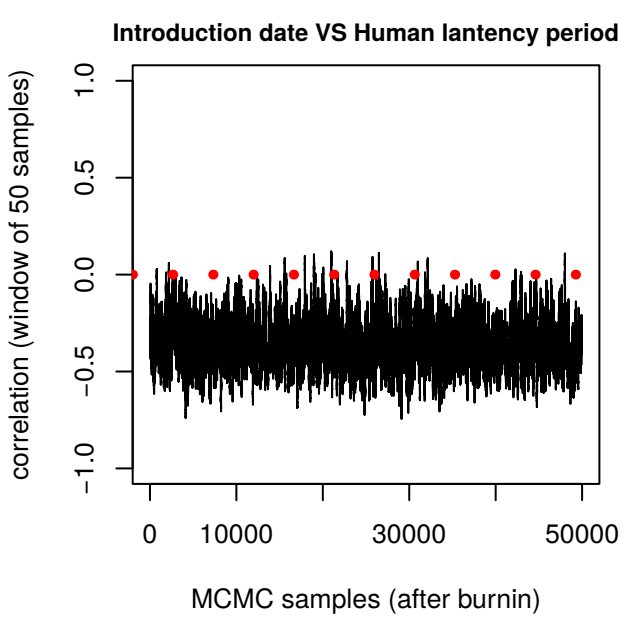
Introduction date VS Human lantency period
correlation (window of 50 samples)
MCMC samples (after burnin)

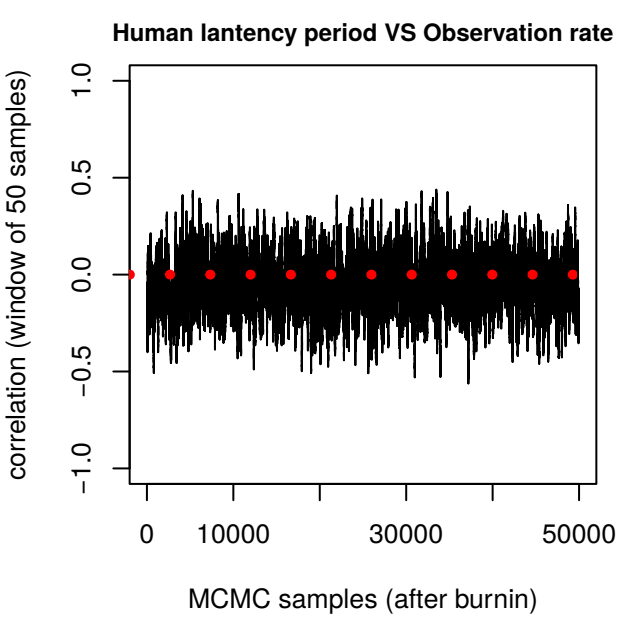
Human lantency period VS Observation rate
correlation (window of 50 samples)
MCMC samples (after burnin)

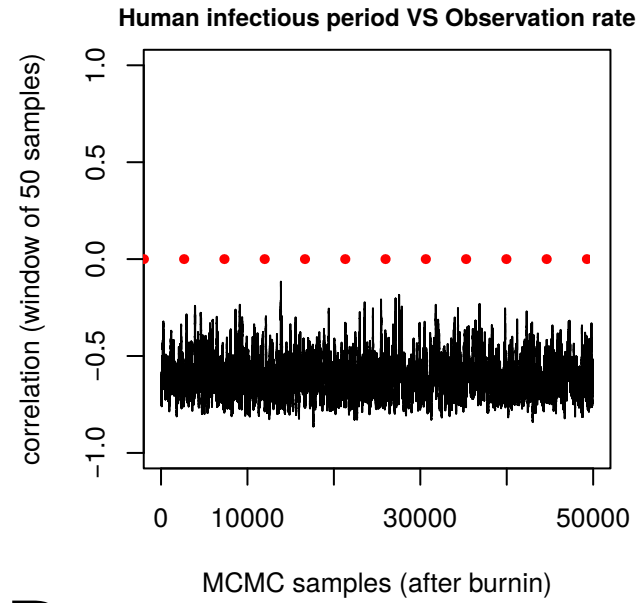
Human infectious period VS Observation rate
correlation (window of 50 samples)
MCMC samples (after burnin)

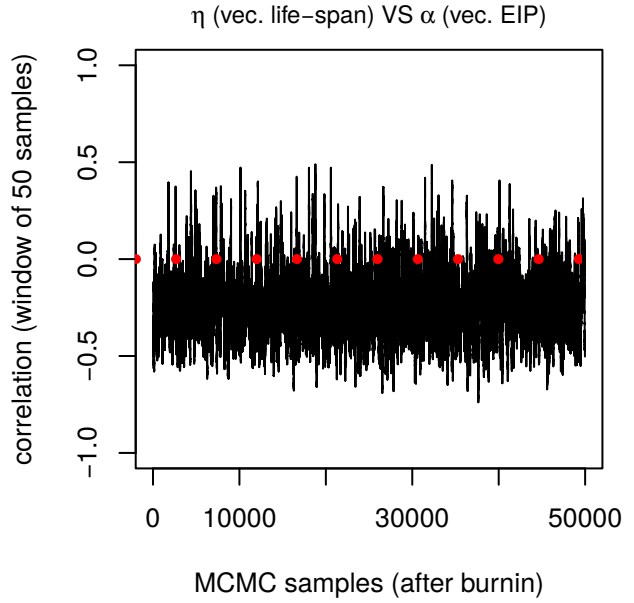
η (vec. life−span) VS α (vec. EIP)
correlation (window of 50 samples)
MCMC samples (after burnin)

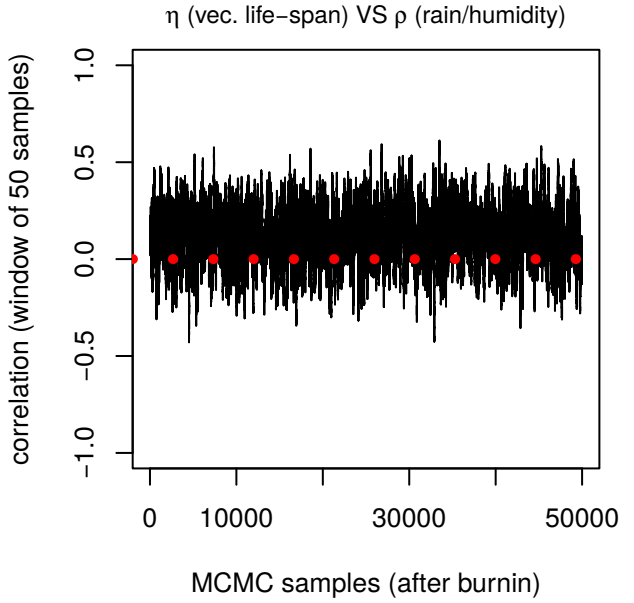
η (vec. life−span) VS ρ (rain/humidity)
correlation (window of 50 samples)
MCMC samples (after burnin)

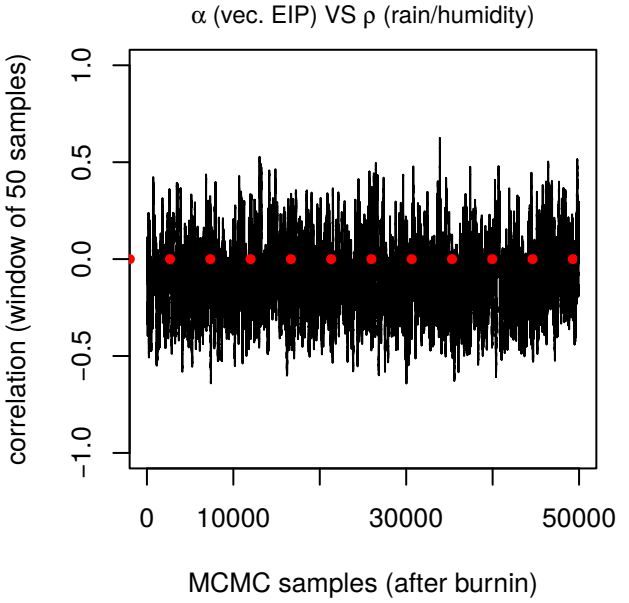
α (vec. EIP) VS ρ (rain/humidity)
correlation (window of 50 samples)
MCMC samples (after burnin)

B

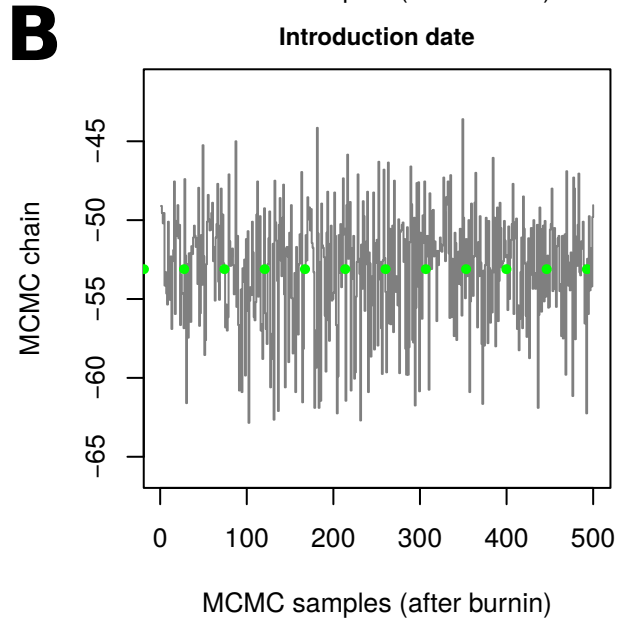
Introduction date
MCMC chain
MCMC samples (after burnin)

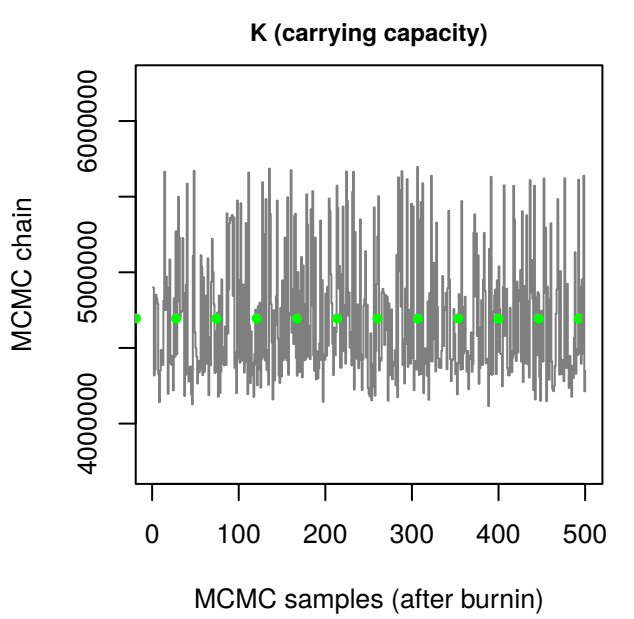
K (carrying capacity)
MCMC chain
MCMC samples (after burnin)

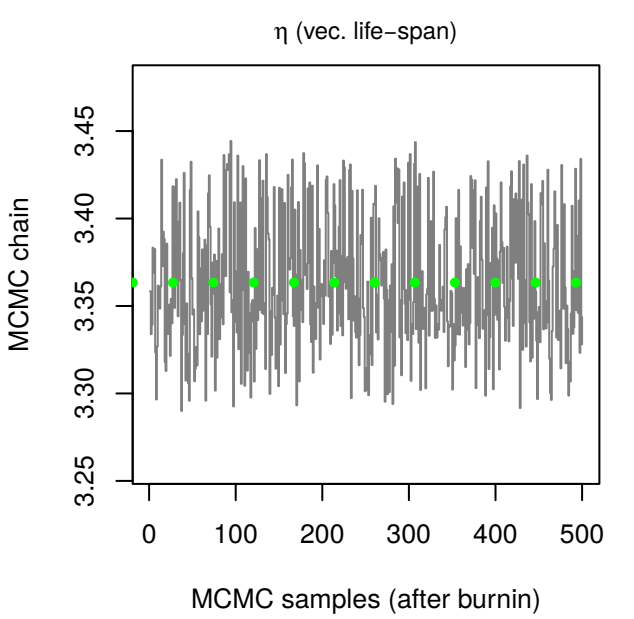
η (vec. life−span)
MCMC chain
MCMC samples (after burnin)

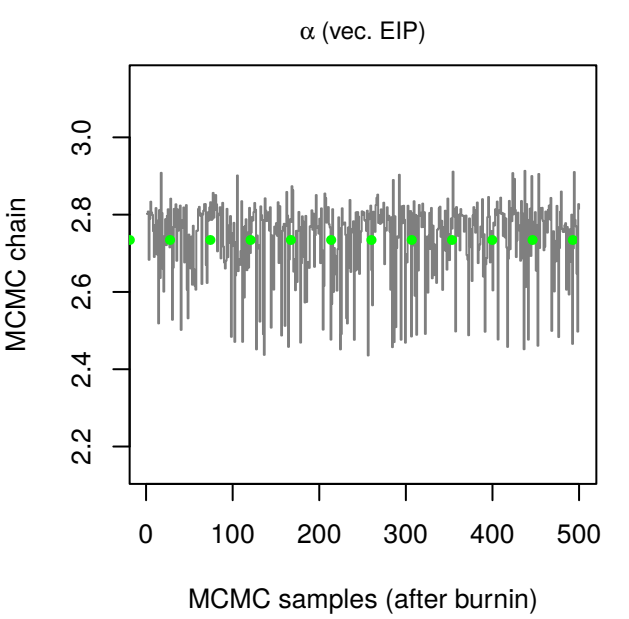
α (vec. EIP)
MCMC chain
MCMC samples (after burnin)

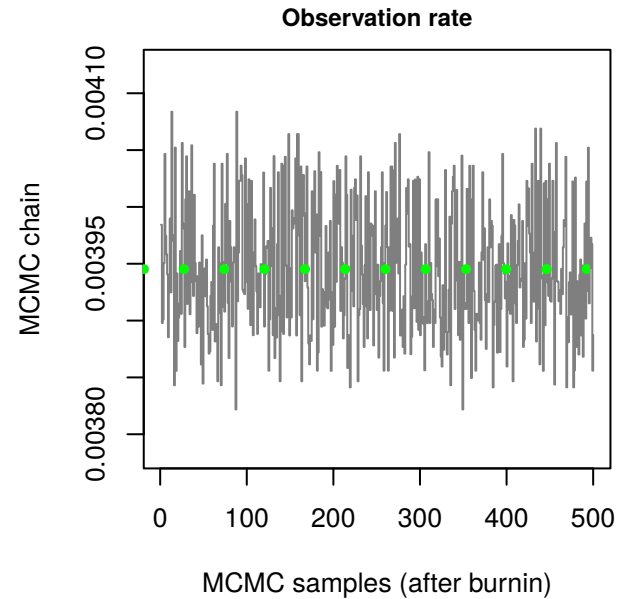
Observation rate
MCMC chain
MCMC samples (after burnin)

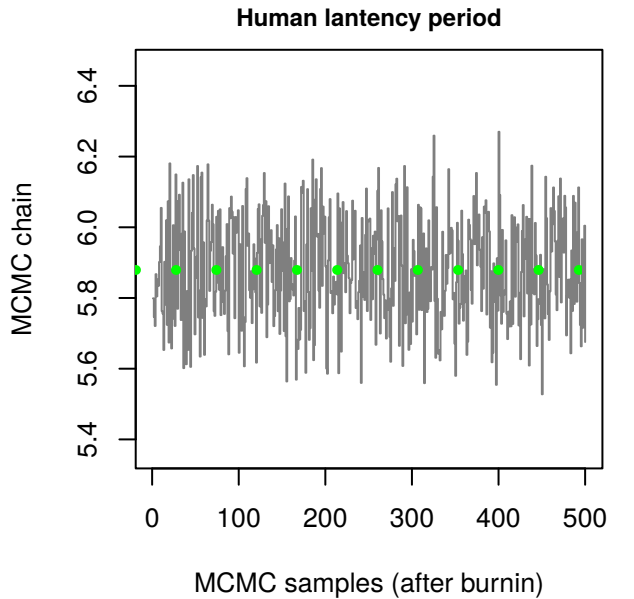
Human lantency period
MCMC chain
MCMC samples (after burnin)

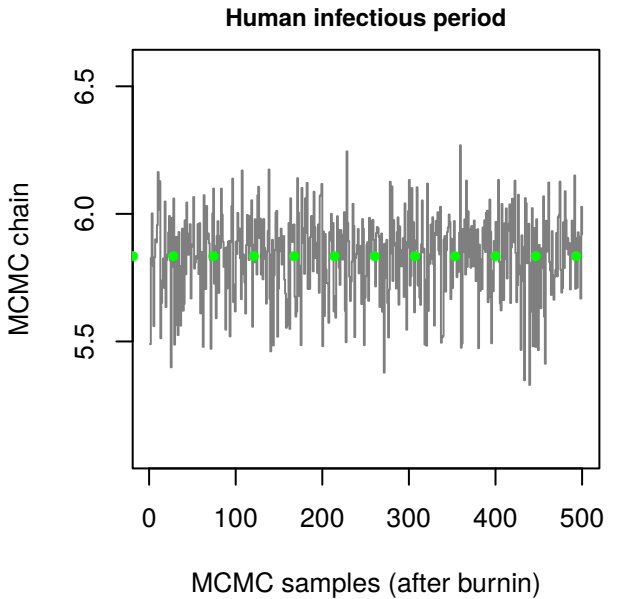
Human infectious period
MCMC chain
MCMC samples (after burnin)

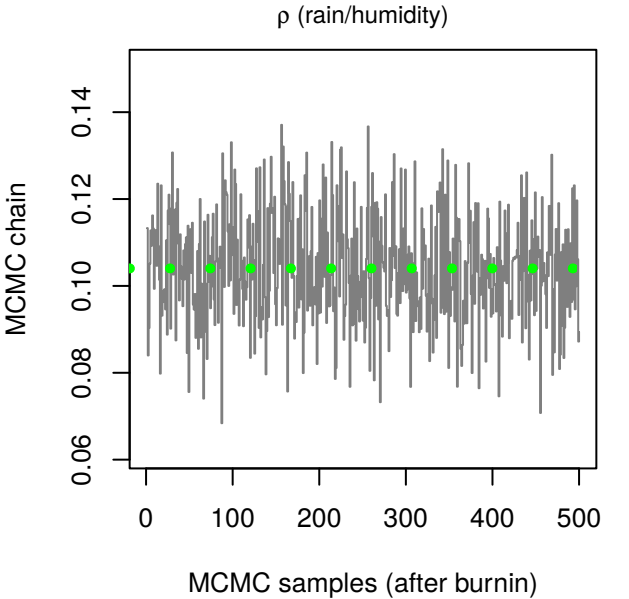
ρ (rain/humidity)
MCMC chain
MCMC samples (after burnin)

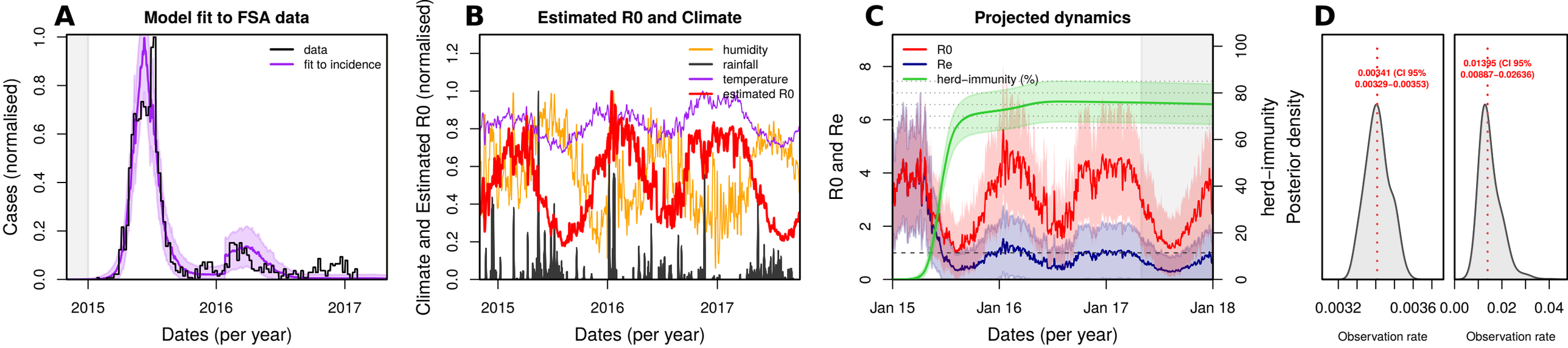
A
Model fit to FSA data
data
fit to incidence
Cases (normalised)
0.0
0.2
0.4
0.6
0.8
1.0
2015
2016
2017
Dates (per year)
B
Estimated R0 and Climate
humidity
rainfall
temperature
estimated R0
Climate and Estimated R0 (normalised)
0.0
0.2
0.4
0.6
0.8
1.0
1.2
2015
2016
2017
Dates (per year)
C
Projected dynamics
R0
Re
herd−immunity (%)
R0 and Re
0
2
4
6
8
herd−immunity
0
20
40
60
80
100
Jan 15
Jan 16
Jan 17
Jan 18
Dates (per year)
D
Posterior density
0.00341 (CI 95%
0.00329−0.00353)
0.0032
0.0036
Observation rate
0.01395 (CI 95%
0.00887−0.02636)
0.00
0.02
0.04
Observation rate